Role of the Intron 13 Polypyrimidine Tract in Soluble Flt-1 Expression

Rebecca I. Roche

Thesis submitted to the faculty of the Department of Biomedical Sciences and Pathobiology, Virginia-Maryland Regional College of Veterinary Medicine, Virginia Polytechnic Institute and State University to fulfill the requirements for the degree of

Master of Science in
Veterinary Medical Sciences

_____

Dr. William R. Huckle, Chair

_____

Dr. Glenda Gillaspy

_____

Dr. John L. Robertson

May 2, 2002
Blacksburg, Virginia

Key words: Angiogenesis, Vascular Endothelial Growth Factor, Flt-1, sFlt-1, RNA Splicing, Polypyrimidine Tract

ROLE OF THE INTRON 13 POLYPYRIMIDINE TRACT IN SOLUBLE FLT-1 EXPRESSION

By

Rebecca I. Roche

(ABSTRACT)

Angiogenesis is the formation of new blood vessels from existing vasculature. Vascular Endothelial Growth Factor (VEGF), a known angiogenic protein, stimulates endothelial cell proliferation and migration via interactions with its receptors, KDR and Flt-1. A secreted form of Flt-1 (sFlt-1), derived from alternatively-spliced RNA, can inhibit actions of VEGF *in vivo*. It has been suggested that alterations in sFlt-1 expression could significantly change the angiogenic VEGF activity. This project focuses on characterizing intronic elements that regulate Flt-1 mRNA splicing. A "wild-type" construct (pFIN13), containing the first 13 exons, intron 13 and exons 14-30 of mouse Flt-1, was shown to produce both forms of Flt-1 mRNA after transfection into HEK293 cells. To gauge the strength of the native splicing signals in intron 13 of Flt-1, a series of point mutations were made in the polypyrimidine tract using pFIN13. After transient transfection, the levels of Flt-1 and sFlt-1 protein and mRNA were compared using quantitative PCR, RNA hybridization analysis, and protein immunoblotting. Results from quantitative PCR showed that purine substitutions were associated with 120 to 350 fold decreases in Flt-1 mRNA (normalized against neo^r), consistent with less efficient splicing. These large decreases in Flt-1 mRNA were accompanied by increases in sFlt-1 mRNA. Modest (20 to 100%) increases in Flt-1 mRNA, reflecting improved splicing, resulted from increasing the uridine complement in the polypyrimidine tract. These results suggest that the wild-type polypyrimidine tract is of intermediate strength and may be a regulatory locus for modulating Flt-1: sFlt-1 ratios.

DEDICATION

This manuscript is dedicated to my father. He was my strength, my courage, my hope, my support and my friend. His spirit will be with me always. With all my courage, hope, and love. Thank you, Dad.

ACKNOWLEDGMENTS

I would like to thank everyone who helped make this goal achievable. Thank you to all my friends and family for their support, encouragement, and love. This has been a daunting task at times and having help by my side has been wonderful. Thank you, Benjamin for being there for me.

Very special thanks go to Dr. Huckle for his encouragement, positive feedback, constructive criticism, knowledge, and time. He is a wonderful advisor and person who went above and beyond to aid in the success of this project. I consider him not only my advisor but a friend as well. I look forward to continuing on under his wing and hope to contribute positively to his personal success and the success of this project.

TABLE OF CONTENTS

LIST OF FIGURES AND TABLES

INTRODUCTION

Angiogenesis is the formation of new blood vessels from the pre-existing vasculature (1). It has been shown to be important in reproduction (2, 3), embryo development (5), and wound repair (1). Alternately, it has been related to diseases such as arthritis (4), diabetes, and neoplasia (1). In normal tissue, endothelial cells are quiescent, but in either physiologic or pathologic processes, they can be stimulated by a number of factors including, but not limited to, ischemia (5), tissue hypoxia (6), cytokines (10, 11), acidic fibroblastic growth factor (aFGF), basic fibroblastic growth factor (bFGF), vascular endothelial growth factor (VEGF), and angiogenin (4).

VEGF is one of the primary angiogenic factors stimulating endothelial cell proliferation and migration (10, 12, 14, 22). VEGF induces endothelial cells to express proteases and plasminogen activators to begin the process of angiogenesis (10). The structure of VEGF is such that it is able to form homo- or heterodimers (11). Other VEGF-related proteins have been found to interact with VEGF through dimerization and/or VEGF receptor use. These receptors are primarily found in the vascular endothelium (11).

Two VEGF receptors, Flt-1 and KDR, belong to the receptor-type tyrosine kinase superfamily, having seven immunoglobulin-like (IgG-like) domains making up the extracellular region, a transmembrane domain, and an intracellular region containing a tyrosine kinase domain divided by a long kinase-insert domain. Mice lacking KDR or Flt-1 undergo early embryonic death, however, phenotypically the vasculature in these animals is distinct (23, 24, 25, 26). KDR-null mice show a deficiency of vascularization caused by a lack of endothelial cell development (23, 24). Mice deficient in Flt-1 develop highly defective vasculature that is unorganized and often contains endothelial cells in the lumen (23, 24, 25).

A secreted form of Flt-1 (sFlt-1) was discovered to negatively affect VEGF signaling. This form is synthesized from an alternately spliced Flt-1 mRNA, and contains the first six IgG-like domains of Flt-1 and a unique C-terminus. This C-terminus is derived from a portion of an intron normally cleaved out of the Flt-1 mRNA

(intron 13). The sequence coding for the transmembrane domain and the intracellular domains of the receptor are not present in sFlt-1. The predicted structure of sFlt-1 implies a VEGF binding receptor that inhibits the cellular response associated with VEGF/Flt-1 and VEGF/KDR interaction (35, 36). It has been suggested that alterations in the levels of sFlt-1 could significantly change the angiogenic activity of tumor-derived VEGF. Therefore, it could be possible that a change in sFlt-1 expression levels could influence the vascularization of tumors.

We hypothesize that the splice recognition sequences of intron 13, especially the polypyrimidine tract, are crucial for the regulation of sFlt-1 expression. In the present study, we explore altering sFlt-1/Flt-1 levels by regulating the splicing event. The intronic splicing elements of intron 13 are classified as U2 dependent. However, the polypyrimidine (PPy) tract is not optimal. It is of moderate length, but contains relatively low uridine content (10:6, C:U). Long continuous stretches of uridinyl residues, a determinant of splice factor protein binding, are not present. Based on previous studies of other PPy tracts, specific base changes were made in the PPy of intron 13. As a result of these changes, alterations in expression levels occurred in both Flt-1 and sFlt-1. Our results suggest that the wild-type polypyrimidine tract is of intermediate strength and may be a regulatory locus for modulating Flt-1: sFlt-1 ratios.

LITERATURE REVIEW

Angiogenesis

Angiogenesis is the formation of new blood vessels from the pre-existing vasculature (1). It has been shown to be important in reproduction (2, 3), embryo development (5), and wound repair (1). Alternately, it has been related to diseases such as arthritis (4), diabetes, and neoplasia (1). In normal tissue, endothelial cells are quiescent, but in either physiologic or pathologic processes, they can be stimulated by a number of factors including, but not limited to, ischemia (5), tissue hypoxia (6), cytokines (10, 11), acidic fibroblastic growth factor (aFGF), basic fibroblastic growth factor (bFGF), vascular endothelial growth factor (VEGF), and angiogenin (4).

Well-regulated angiogenesis is important for normal reproductive function. During foliculogenesis, the dominant follicle develops complex vasculature stimulated by angiopoietins and VEGF (2). In this case, VEGF and angiopoietin upregulation is caused by hypoxia. The corpus luteum is also dependent upon new capillary vessel formation (3). In the uterus of cycling females, vascularization occurs with each menstrual cycle as the endometrium prepares for implantation of the ovum (2). This process is thought to be partially under hormonal control (3). Vasculogenesis, the differentiation of vascular tissues, and angiogenesis both occur very early in fetal development. High levels of angiogenic growth factors (aFGF, bFGF, VEGF, and placenta growth factor [PlGF]) and their receptors are expressed in the human placenta (70). Vascularization of the placenta begins with *de novo* formation of capillaries. The number of capillaries increases through branching until the end of the first trimester (70). During this period, VEGF and its receptor KDR are expressed at high levels. However, from 26 weeks to term, PlGF and Flt-1 are dominant, as non-branching angiogenesis takes place developing a new type of villous (70).

In the process of retinal development, regulation of VEGF function can lead to either a functional eye or blindness. Normally, the astrocytes and neuronal precursors become spread out as the retina develops. As this occurs, the cells are pushed further away from the existing vasculature and hypoxic conditions ensue. VEGF is produced in these hypoxic cells, which in turn begins the angiogenic process. New blood vessels

form, and hypoxia is lessened. Through a feedback loop, VEGF expression is then slowed as the cells respond to the presence of oxygen and other nutrients supplied through the vasculature. However, in retinopathy of prematurity, the hyperoxygenated incubators cause the astrocytes to decrease VEGF production and retinal vascular development is slowed or completely stopped. Once the infant is removed from this super-oxygenated environment, the astrocytes sense relative hypoxia and VEGF is produced at an abnormally high level. This, in turn, causes rapid uncontrolled angiogenesis leading to blindness. The hyperproliferation of blood vessels due to the overexpression of VEGF in other ocular diseases (diabetic retinopathy [7, 16] and macular degeneration) has also been shown to lead to blindness (11).

In cancer, high blood vessel density has been correlated to tumor growth rate and high metastatic potential (17, 18, 19, 20, 21). In general, tumors with a higher intratumoral microvascular density have a higher potential to metastasize by spreading more cells that are already of the angiogenic phenotype (21). Tumors with more vasculature have more contact area with the blood stream, a greater number of cells expressing angiogenic mitogens, and a greater ability to metastasize. However, this may not be the case across all tumor types. When integrated with other case-specific factors, tumor vascularity may serve as a prognostic tool for the outcome of the patient.

Various factors indicate a requirement for the vascularization of solid tumors for growth beyond 1-2 mm^3, a hypothesis articulated by Judah Folkman in the 1970's (7, 8, 9, 24). According to Lewin (8), this size reflects the maximal thickness of tissue through which oxygen and other nutrients can diffuse. Growth is outweighed by apoptosis and necrosis beyond this size. Tumor growth and expansion is dependent not only on the perfusion of blood but also on the paracrine stimulation by several growth factors and proteins provided by the new vascular endothelium. The balance of positive and negative angiogenic factors released by the tumor determines if the tumor remains quiescent or converts to the angiogenic phenotype (4). Environmental factors and genetic changes that either increase angiogenic factors or decrease inhibitors arbitrate this transformation. It is a multistep process beginning with the binding of growth factors (VEGF and others) to their receptors leading to the breakdown of the extracellular matrix by proteases

produced by activated endothelial, tumor, and inflammatory cells. This change in environment allows the endothelial cells to proliferate, invade, and migrate towards the angiogenic stimulus. Once at their new location, tube formation begins with cellular reorganization and tight junction development. The new vasculature becomes operational with a connection to the existing blood vessels (7). Many tumor types over express VEGF (10), including hematopoietic malignancies (9), glioblastomas (20), malignant melanoma (19), as well as some carcinomas and osteosarcomas (17).

Vascular Endothelial Growth Factor (VEGF)

Due to the correlation of tumor vascularity and severity, researchers have been focusing cancer therapy on tumor endothelial cells. This has been advantageous for several reasons. Tumor endothelial cells tend to be more accessible than other tumor cell types, and yet they allow increased target specificity and therefore decrease treatment side effects. They are also thought to be more genetically stable than tumor cells, and therefore are less likely to develop resistance to drug treatments. Finally, they provide a common target for all solid tumors regardless of histologic type (7).

Blood vessel growth is strongly influenced by VEGF and its receptors (10, 12, 14, 22). The effects of VEGF are directed almost exclusively toward the vascular endothelium (11). Through the use of murine models, it has been determined that the loss of one allele for VEGF creates severe developmental vascular deformities and leads to early embryonic death (10, 11, 14, 15). Several splice variants of VEGF have been discovered ranging in size from 121 to 206 amino acids. These VEGF isoforms differ in their affinity for heparin (10). One of the first forms discovered was purified via heparin binding (13). Location and level of expression also differ across VEGF type, with 121, 165, and 189 being most abundant. VEGF-A isoform 165 is regarded as the most abundant form and will be referred to as VEGF here. It is a secreted molecule, which mediates endothelial cell growth and angiogenesis (13). VEGF induces endothelial cells to express proteases and plasminogen activators to begin the process of angiogenesis (10). The structure of VEGF is such that it is able to form homo- or heterodimers (11). Other VEGF-related proteins have been found to interact with VEGF through

dimerization and/or overlaping receptor use. Some of these are close VEGF homologues (PlGF, VEGF-B, -C, -D, and -E), while other endothelial growth factors (PDGF – platelet-derived growth factor, and FGF's – fibroblast growth factors) activate distinct families of receptors (68). Unlike VEGF, bFGF and aFGF lack a hydrophobic signal peptide, a requirement in classical secretory pathways for extracellular transit. These other growth factors have been found to serve alternate functions that will not be discussed further here.

VEGF Receptors

KDR and Flt-1

Several receptors exist for VEGF. The best characterized of these are Flt-1 (*fms*-like tyrosine kinase, VEGFR-1), and KDR (kinase insert domain containing receptor, VEGFR-2; the human homologue of murine Flk-1, fetal liver kinase). Both belong to the receptor-type tyrosine kinase superfamily (30). They are structurally similar with seven immunoglobulin-like domains making up the extracellular region, a transmembrane domain, and an intracellular region containing a tyrosine kinase domain divided by a long kinase-insert domain (23, 25, 27, 34) (Figure 1). In the case of Flt-1, the first, second, and third immunoglobulin-like domains are required for ligand binding, and the fourth domain is involved in receptor dimerization (30, 31, 32, 33, 34). When VEGF binds KDR and/or Flt-1, a conformational change occurs. This is followed by dimerization of the receptors (either homo- or hetero-) and autophosphorylation (27). This activates a signal transduction pathway within the cell. Through *in vitro* work, *ras* GTPase-activating protein, *src* protein kinases, phospholypase Cγ and elements of the mitogen-activated protein kinase pathways are suspected members of the VEGF/KDR signal transduction pathway (25, 27). Crossover is suspected between the VEGF/KDR pathway and the VEGF/Flt-1 pathway, but because the two receptors trigger different cellular responses, the likelihood of the pathways being identical is poor (27, 28).

Several sources cite KDR as the dominant VEGF receptor with respect to mitogenic cellular responses. Early embryonic death has been shown in both KDR (-/-) and Flt-1 (-/-) mice (23, 24, 25, 26). However, the resulting phenotypes of these mice are

Receptor Structure

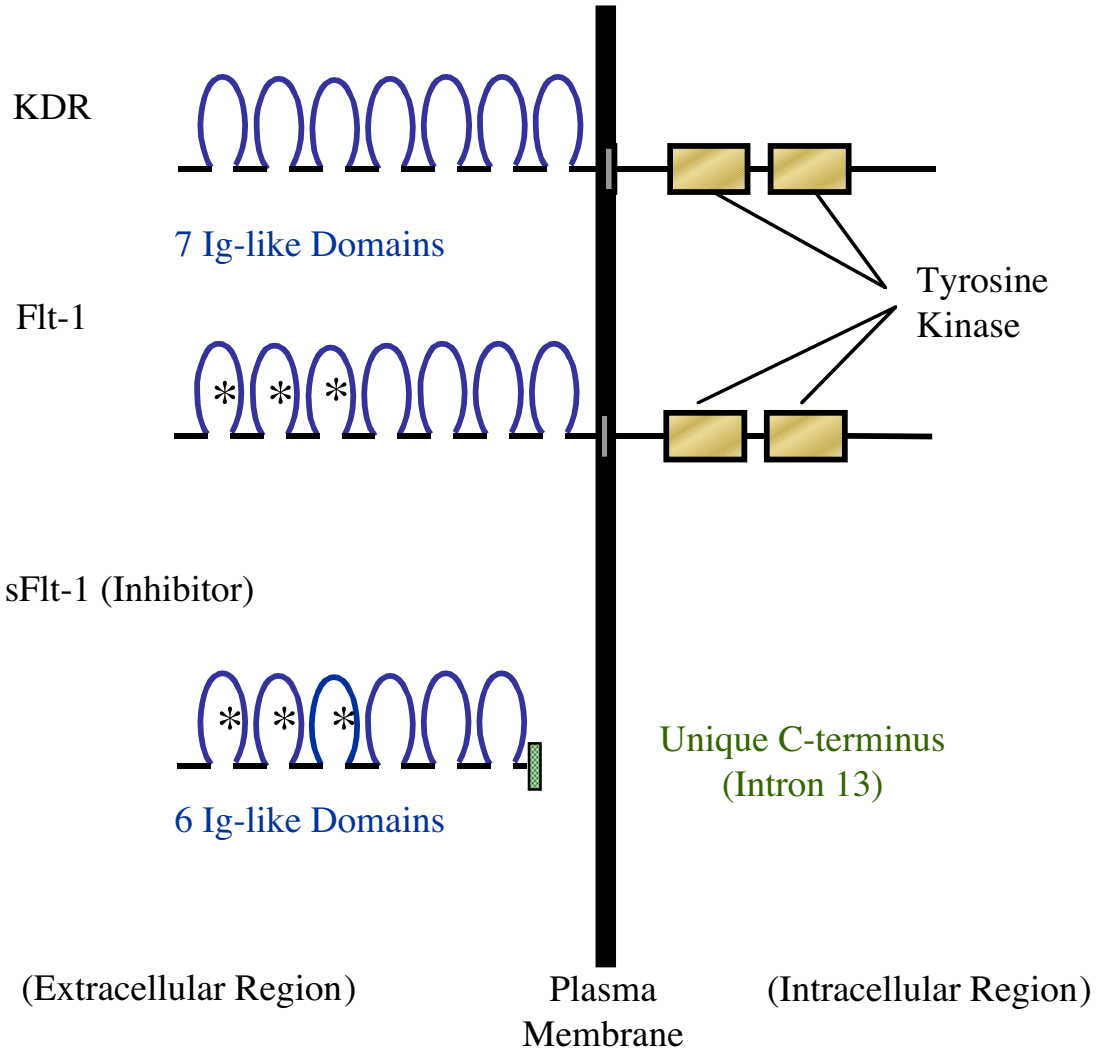

Figure 1. Receptor protein structure. Although structurally similar, Flt-1 and KDR elicit different cellular responses due to varying ligand binding. Alternate splicing events lead to 2 different protein structures: Flt-1, a transmembrane receptor, and sFlt-1, a secreted receptor that is structurally similar to Flt-1 up to Ig-like domain 6. Because sFlt-1 lacks the transmembrane and intracellular regions, it does not elicit a VEGF response and has been characterized as a VEGF inhibitor. VEGF binding domains are marked (*).

different. Studies have shown a deficiency of vascularization due to defective endothelial cell development in the KDR (-/-) mice (23, 24). In the Flt-1 (-/-) mice, however, embryos will develop vasculature through endothelial cell differentiation. This vasculature is highly abnormal and unorganized with an overgrowth of endothelial cells crowding the lumen (23, 24, 25). Cells grown *in vitro* expressing either KDR or Flt-1 also show differences in cellular morphology when stimulated with VEGF. Cells expressing KDR display cytoplasmic protrusions and ruffled edges after five minutes of treatment, and major changes in shape including pili after 15 minutes (28). Those expressing Flt-1, when challenged with an equal amount of VEGF, reveal no response to VEGF through cell morphology or cytoskeletal reorganization. Upon equal application of VEGF, a greater tyrosine kinase activity occurs in the KDR receptors than the Flt-1 receptors (23, 25, 28). However, the Flt-1 receptor, though less abundant, has a greater VEGF binding affinity (23, 25, 26, 28, 34). Dissociation constants for VEGF binding by the two receptors vary by a great deal, with Flt-1 ranging from 15-100 pM and KDR ranging from 400-800 pM (12, 25, 28, 34). One other difference between the two receptors is that Flt-1 seems to be present in endothelial cells and possibly the monocyte/macrophage population (26). KDR, on the other hand, has been found in endothelial cells, fetal liver cells, and pancreatic duct cells (28).

sFlt-1

A secreted form of Flt-1 (sFlt-1), derived from alternatively spliced RNA, has also been discovered. cDNAs encoding this receptor was isolated from a human umbilical vein endothelial cell (HUVEC) cDNA library (35, 36). The sequence of sFlt-1 was predicted to be identical to that of Flt-1through the 6th Ig-like domain. sFlt-1 cDNA was proposed to contain a portion of an intron that is normally spliced out of the full-length receptor (35) (Figure 2). The suspicion of an uncleaved intron was increased when a common intron donor site was found (AG) and confirmed with genomic PCR analysis and DNA sequencing (35). Originally, this intronic sequence was believed to be meaningless, as was the trend with most intron sequences. However, it is now believed to be of some importance because the intron 5' end is highly conserved between mice and

Flt-1 and sFlt-1 Splicing

DNA

Flt-1 mRNA

sFlt-1 mRNA

Figure 2. The alternate splicing event. Flt-1 mRNA is spliced traditionally excluding all introns. sFlt-1 is spliced traditionally up to exon 13. A fragment of intron 13 remains in the sFlt-1 mRNA.

humans (12, 37). Flt-1's seventh immunoglobulin-like domain, in addition to the transmembrane and intracellular domains, are predicted to be missing from the structure of sFlt-1, replaced by a unique C-terminus (35). The predicted structure of sFlt-1 implies a VEGF binding receptor that inhibits the cellular response associated with VEGF/Flt-1 and VEGF/KDR interaction (35, 36). sFlt-1 is suspected to maintain quiescence in monolayers of confluent endothelial cells, terminate angiogenesis and vascular permeability as a feedback mechanism, and, in tissues that are normally avascular, prevent blood vessel growth. It is believed to form inactive heterodimers with KDR and Flt-1 and serve in a dominant-negative function (36, 38) or, when present in excess over KDR or Flt-1, soak up much of the available VEGF (35).

It has been suggested that alterations in the levels of sFlt-1 could significantly change the angiogenic activity of tumor-derived VEGF. It is possible, therefore, that a change in sFlt-1 expression levels could influence the vascularization of tumors. Expression of the sFlt-1 receptor has been shown in the adult kidney, liver, and uterus (38). One theory of regulation correlates the unusually hypoxic environment of the placenta and the varied expression of both Flt-1 and sFlt-1 during pregnancy (38). Both Flt-1 and sFlt-1 expression was found to change in the placenta of late gestation mice. However, Flt-1 expression was reported to decrease while sFlt-1 expression was reported to increase (38). Using ratios obtained via northern blotting, He *et al*. (38) reports this as a possible mechanism for the regulation of VEGF activity. In the typical cycling human female, Flt-1 and KDR levels have been found to be relatively stable throughout the entire menstrual cycle (39). However, sFlt-1 expression follows a pattern that peaks at the mid-proliferative phase and troughs during the early-secretory phase (39). Hypoxia appears to be partially responsible for this regulation of sFlt-1 here as well. One study showed a brief increase in sFlt-1 but a sustained increase in full-length Flt-1 mRNA levels in HUVECs incubated with conditioned media from C6 (derived from rat glioblastomas) cells under hypoxic conditions (41). Variation in Flt-1 and sFlt-1 expression has been shown in reproduction. If this knowledge could be applied to tumors, the possibility of inhibiting tumor vascularization is greater.

VEGF as an Anti-angiogenic Target

Due to its negative influence on VEGF signaling, exogenous sFlt-1 has been studied in correlation with tumor growth. Immunodeficient mice were injected with HT-1080 cells transfected with a plasmid containing sFlt-1 or a plasmid only control. Upon histologic examination of the lungs, seven out of nine contained tumor nodules in the control group, while only one of nine in the sFlt-1 group expressed nodules (40). This indicates that even transient expression of sFLt-1 has a negative effect on tumor growth (specifically HT-1080 lung metastasis). In another study, stably transfected cell lines expressing sFlt-1 at two different levels and a plasmid only control were injected into nude mice. The control group experienced rapid tumor growth. The animals injected with the lower expression level of sFlt-1 grew significantly smaller tumors while those injected with the higher sFlt-1 expression line were even smaller (40). This study demonstrates that the higher, more consistent sFlt-1 levels slowed tumor growth. In another study using an A375v human melanoma xenograft model, tumors derived from tumor cells stably transfected with sFlt-1, reached only 18-43% of the size of the tumors in the controls (42). Another difference was the reduced vascular density in the experimental line (42). In a third study using a murine model of ovarian carcinomas, a dose/treatment regime was tested using adenovirus-mediated sFlt-1 overexpression (43). Implantation and growth of tumors, in addition to survival time, was measured in two different experiments. In the first, BALB/c nude mice were injected with either sFlt-1-infected or uninfected tumor cells. Mice that received the infected cells showed significantly smaller tumors than the uninfected controls. In the second experiment, CB17 SCID mice were implanted with ovarian tumor cells and then dosed with either vector-only control cells or sFlt-1 expressing cells. The sFlt-1 treated mice survived significantly longer than the control animals (43).

Based on the association between tumor VEGF, vascularity, and disease progression, VEGF and its receptors have become targets of antiangiogenic therapy. Currently there are two forms of antivascular therapy being tested in the treatment of neoplasia: antiangiogenic therapy and vascular targeting. These treatments can be further divided into several groups: drugs that inhibit the breakdown of the extracellular matrix,

those that have endothelial cell growth inhibition, angiogenic blockers, endothelial-specific integrin signaling inhibitors, and those with non-specific modes of action. Vascular targeting has been assisted through the development of antibodies that target specific markers expressed on the surface of endothelial cells (7). Because the VEGF mediated signaling cascade is still somewhat unknown and possibly involved in numerous other signaling events, targeting members of the cascade has proven difficult. However, an attempt has been made to develop an antagonist to cyclic adenosine monophosphate (cAMP) and inhibitors of protein kinase C (45). Neutralizing antibodies have been developed against VEGF (22) and KDR (25). One of these is currently undergoing human clinical trials. An artificially truncated form of the KDR receptor has been created with hopes that it will function similarly to sFlt-1 and in turn block the actions of VEGF (40). Antisense technology has been used to stably transfect a cell line to harbor antisense-VEGF cDNA (22). Both of these methods reduce the amount of expressed VEGF.

As with most treatments, these have their drawbacks. When treating patients with angiogenic therapies, there is often a problem with achieving a non-desired systemic effect in addition to a localized one. A safety feature of the VEGF target is that its effects are localized to endothelial cells. However, signal transduction pathways are not exclusive and therefore could lead to increased problems with associated disease. For example, if an elderly patient develops a tumor but also has a history of poor peripheral circulation due to age or disease, attacking angiogenic proteins to treat the tumor could also increase the patient's distal circulatory problem (16). Non-biological inhibition of VEGF is also likely to cause negative side effects. These could include ischemia, abnormal menstrual cyclicity (16), and abortion. One solution to these problems is the use of a viral vector to administer the treatment. A replication-deficient adenovirus vector is being tested for use in the enhancement of local control of and systemic immunity against tumors (44). This system allows for a more targeted treatment of the tumor, for example, by inhibiting angiogenesis locally (44). Another idea along these lines is the incorporation of sFlt-1 into the viral vector so when expressed, it will locally sequester VEGF directly or through a dominant-negative heterodimerization with Flt-1 or

KDR (44). A drawback to the modified adenovirus vector as a treatment is the possibility of induction of an immune or inflammatory response (16). Other problems arise with administration of these treatments. Often there is an occurrence of vasodialation and hypertension during short-term administration.

Because of problems associated with pharmacological treatments, research is beginning to trend toward utilizing endogenous treatments. sFlt-1 is an example of a biological inhibitor for the VEGF system. Therefore, regulation of this receptor could prove beneficial as an anti-tumor therapy. Regulation of the splicing balance between Flt-1 and sFlt-1 is not unique. In a similar alternative splicing situation of the mRNA's encoding the membrane-bound (m) and secreted (s) forms of IgM heavy chain (μ), there is a balance between cleavage-polyadenylation and splicing (64). As B cells mature, there is a shift in which of these forms is produced. The same region of DNA encodes for both μs and μm forms. The μs mRNA is produced by early cleavage-polyadenylation, while μm is produced by splicing the exons and polyadenylating further down stream (64). Early in B cell growth, the μm form predominates, while in mature plasma cells, μs is favorably produced. In an experiment to examine regulation, both sequences coding for the events were mutated. In each case, a stronger sequence was substituted for the wild type and combined with either the wild type or a weaker substituted sequence. It was determined that both the polyadenylation and splicing sites were sub-optimal but balanced (64). Therefore, improving the polyadenylation site caused more mRNA to be cleaved and polyadenylated than was spliced. The reverse was also shown to be true. This sub-optimal condition is found frequently and is often an important part of the regulatory mechanism (64, 66).

Splicing

RNA splicing is a multi-step process where the pre-mRNA interacts with several components of the spliceosome (Figure 3). First, the U1 snRNA (small nuclear RNA) interacts with the 5' splice site through RNA-RNA base pairing (47, 48, 49, 51, 54, 67). Then U2AF (U2 snRNP auxiliary factor) and SF1 (splicing factor 1) recognize the polypyrimidine tract and 3' splice site (47, 49, 54). Once this recognition occurs, the

General Splicing Mechanism

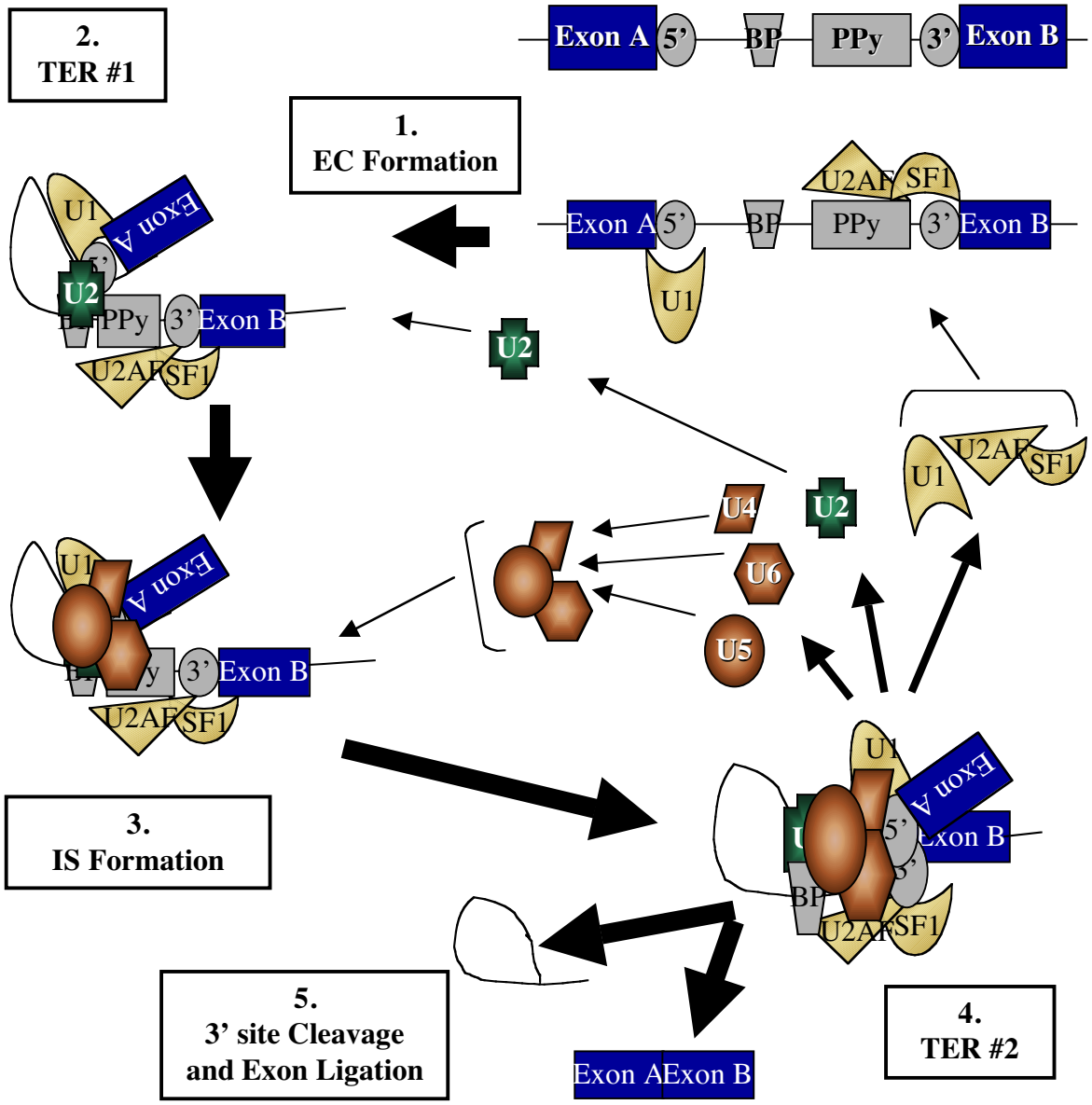

Figure 3. A simplified splicing mechanism. Step 1. U1 snRNA, U2AF^{65} and SF1 binding to pre-mRNA at the 5' splice site, the polypyrimidine tract (PPy) and the 3' splice site, respectively, forming the Early Complex (EC). Step 2. The EC and the U2 snRNP interact to yield the pre-spliceosome and the 1st transesterification reaction (TER 1) takes place coupling the 5' splice site to the branch point (BP). Step 3. The pre-formed complex containing U4, U5 and U6 binds to the EC to make the immature spliceosome (IS). Step 4. Reorganization of the IS occurs rendering the spliceosome functional and the 2nd transesterification reaction (TER 2) takes place cleaving the 3' splice site and ligating the exons.

early complex (EC) is formed. The EC and the U2 snRNP interact yielding the prespliceosome. Following this, the first transesterification reaction takes place hydrolizing the 5' splice site and coupling it to the branch point adenosine (49, 50, 54). This interacts with a preformed tri-snRNP containing U5, U4, and U6 to make the immature spliceosome (49). The complete spliceosome is formed after some rearrangements of the immature spliceosome, which render it functional. This then interacts with the branch point again to yield the second transesterification reaction (49). This time, the 3' splice site is cleaved and the exons are ligated (48, 50).

Consensus sequences for the splice sites have been described (Figure 4). This consensus of a U2 dependent intron (GU/AG) has been well established (47, 54, 72). The 5' splice site consensus can be extended to read cAGGTRAGt (where R is a purine [either A or G], and the lowercase letters occur 46% of the time), but the consistency of this is reduced (47). The consensus for the 3' splice site is, when extended, NCAGg (where N represents any nucleotide) (47, 48). The branch point sequence for mammalian species is equally agreed upon, but is more variable in composition. Reed and Palandjian (54) published the sequence to be YNRAY where Y represents a pyrimidine, R represents a purine, and N represents any nucleotide. Several others have published similar sequences, but this is the most liberal (47, 52, 53, 54, 66, 67). Splice site strength may be predicted by its closeness in sequence to the consensus (48, 64). This strength, through protein binding affinity, is an important locus of regulation (49).

Influence of the Polypyrimidine Tract

The 5' and 3' splice sites and the branch point are believed to be the principal determinants of where splicing occurs (46, 47, 54). There are, however, several papers that present information to support the influence of the polypyrimidine (PPy) tract on splicing efficiency. Several references include the PPy tract in the 3' splice site, but it will be treated as a separate entity here. The PPy tract is essential for the efficient recognition of the 3' splice site and branch point utilization (55). In addition to SF1, there is a 65kDa subunit of the spliceosome ($U2AF^{65}$), which is thought to bind the PPy tract (49, 50, 56). This protein influences the interaction of serine-arginine rich proteins

Intronic Splicing Elements

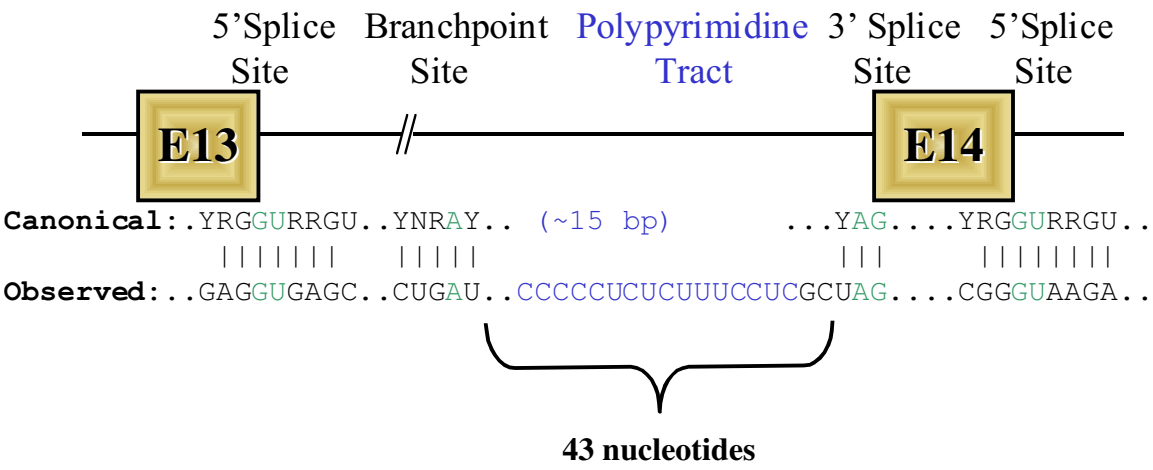

Figure 4. Intronic splicing element identification. Comparison of the intronic splicing elements of intron 13 and the U2 dependent intron consensus sequences.

with the pre-mRNA (50). The actual content and length of the PPy is variable. Frequently, the tract will be made up of varying C/U combinations. Often it will have a stretch that reads UCUUC or UUCU/C that would allow for biding of a polypyrimidine tract binding protein (PTB) (56, 59). This protein was originally thought to be necessary for splicing, but now appears to have an inhibitory effect (55, 56, 59, 60). These proteins are thought to be loci of post-transcriptional regulation of gene expression (60, 63). When sequence modifications are made to the PPy tract that inhibit binding of these proteins, it has been shown that splicing efficiency is also reduced (61, 62, 63). Strong PPy tracts are also often U-rich (55). These stretches would allow for binding of HnRNP C (heterogeneous ribonucleoprotein C), which requires five consecutive uridines to bind (55). In several cases, it has been found that strong PPy tracts can augment or replace the effect of a weak branch point and *vice versa* (52, 55, 57). Mutational analysis of the PPy tract has shown the PPy tract is responsible for determining the location of the branch point and the 3' splice site, and plays a role in the regulation of splice site choice in alternative splicing (55, 65, 66). Additionally, it was determined that in the early events of pre-mRNA splicing, the PPy tract was essential for stable splicing complex formation (55, 67). Mutants were made where the PPy tract was replaced by linker sequences. In these situations, no complexes were formed and only full length RNA was apparent in the gradient fractions, showing no cleavage occurring (67). This particular study also showed that the existence of the 3' splice site dinucleotide enhanced the splicing efficiency but was not necessarily required for splicing (67).

An alternate approach to treating with a recombinant receptor or ligand cDNA or drug is to manipulate the RNA processing event to change expression levels internally. This project focuses on a novel way to change VEGF receptor expression levels, the splicing mechanism of sFlt-1. It is hypothesized that the splice recognition sequences of intron 13, specifically the polypyrimidine tract, are crucial for the regulation of sFlt-1 expression. At this point in time, there are no published documents to our knowledge that address this issue specifically with intron 13.

MATERIALS AND METHODS

The experimental section of this project is comprised of three parts. Part I includes obtaining genomic sequences and creating a "wild type" construct to serve control purposes. Part II is the construction of the intermediate vector for ease of handling the mutations and creating the mutations themselves. Part III contains the methods for testing the mutations *in vitro* through transfection into Human Embryonic Kidney (HEK) 293 cells and harvesting of materials for quantitative PCR, RNA hybridization analysis, and protein immunoblotting.

Part I: Primary Sequence Information and "Wild-Type" Construct Preparation

Before mutations could be made and tested, preliminary information was needed. Clones containing intron 13 had to be obtained and subcloned to be easily handled. Sequencing of this region provided information about the splicing elements. And finally, a construct had to be created that would produce both Flt-1 and sFlt-1 forms. Appendix A contains primer sequences. Appendix B contains information about kits commonly used. Appendix C includes reagent composition and equipment information. All restriction endonucleases and DNA modifying enzymes were obtained from New England Biolabs (NEB) unless otherwise stated.

Subcloning and Sequencing of Genomic Clones

Genomic clones containing intron 13 in its entirety were obtained by screening a mouse Bacterial Artificial Chromosome (BAC) library (RPCI-23) with a fragment of the 5' end of intron 13 as described (75). One μg of purified BAC DNA was digested with either *EcoR*I (20 units with 1x NEBuffer *EcoR*I) or *Hind*III (20 units with 1x NEBuffer 2) in a reaction volume of 20 μl at 37^{o}C for 1 hour. Digests were fractionated on a 1% agarose gel (1% agarose [w/v] in 1x Tris-Borate-EDTA [TBE]), stained with ethidium bromide (EtBr; 1.5 μg/ml in ddH_2O), and viewed by a ultra-violet transilluminating light box. Molecular size markers (λ-*Hind*III plus ϕX 174-*Hae*III, Life Technologies^{TM}) were also included on the gel for size comparison purposes. Fragment groups (2.0-3.0, 3.0-4.5,

4.5-9.0 and >9.0 kb) were then cut from the gel, purified by adsorption to silica beads (QIAEX II Gel Extraction Kit), and eluted with 20 μl 1x Tris-EDTA (TE).

Separately, pLitmus 38 (NEB) was digested with either *EcoR*I or *Hind*III (as described above) and dephosphorylated by addition of 10 units of Calf Intestinal Alkaline Phosphatase (CIP) and additional incubation at 37°C for 1 hour. Purified fragment pools (approximately 100 ng DNA/20 μl ligation reaction) were combined with gel purified linearized, dephosphorylated pLitmus38 (50 ng) and ligated with 1 unit of T4 DNA Ligase (Life Technologies™) overnight at room temperature. Null ligation mixtures were also set up containing vector only. Ligation mixtures (3 μl) were then transformed into a 50 μl suspension of chemically competent DH5α cells (Subcloning Efficiency™, Life Technologies™) on ice for 30 minutes. The cells were then heat-shocked at 37°C for 20 seconds before returning to ice for 2 more minutes. Nine hundred and fifty μl of S.O.C. medium (Life Technologies™) was added to the cells and incubated at 37°C for 1 hour. One hundred μl of this mixture was then spread onto a 100 mm LB-amp plate (Luria-Bertani [LB] agar plus ampicillin at 0.1 mg/ml). Plates were then incubated overnight at 37°C.

Multiple colonies were picked from each plate and inoculated into a 1ml LB-amp broth culture (LB broth plus ampicillin at 0.1 mg/ml). These were then incubated overnight at 37°C with shaking (250 rpm). Two hundred μl of each LB-amp culture was removed to 1.5-ml tubes and centrifuged (14,000 x g, at room temperature) for 5 minutes. The supernatant was aspirated and the cells were resuspended in 100μl 1x TE and heated at 95°C for 5 minutes. One μl of the TE lysate was then used in a polymerase chain reaction (PCR) for screening purposes. Clones were screened for the presence of either the exon 13/intron 13 junction (BH205/BH204) or exon 14 (BH206/BH220) by four stage PCR (Appendix E, Program 1). Each reaction contained final concentrations of 0.25 μM for each primer, 200 μM dNTPs*, 1.5 mM $MgCl_2$*, 0.5 units *Taq* DNA polymerase*, and Tris HCl based buffer* (containing ammonium sulfate, KCl, and $MgCl_2$ optimized for highly specific binding, pH 8.7 at 20°C) (* are contained within 1x *Taq* PCR Master Mix, QIAGEN) and was brought to 20 μl with DNase/RNase free

water. Reaction products were fractionated on 2% agarose gel and stained as previously described.

LB-amp cultures that gave rise to products of anticipated size for the exon 13 / intron 13 junction (321 bp) or exon 14 (60 bp) were streaked onto LB-amp plates and incubated overnight at 37°C. One well-isolated colony per plate was used to inoculate a 100 ml LB-amp culture and was incubated overnight at 37°C with shaking (250 rpm). A 350 μl sample from each 100 ml culture was mixed with 350 μl of 50% glycerol and frozen at –70°C for archival purposes. The balance of each culture was centrifuged at 6,000 x g for 15 minutes. The supernatant was decanted, and the pellet resuspended in 4 ml of 50 mM Tris-Cl (pH 8.0), 10 mM EDTA, and 100u g/ml RNase A. Four ml of lysis buffer (200 mM NaOH and 1% SDS [w/v]) was added and incubated at room temperature for 5 minutes. Four ml of chilled neutralization buffer (3.0 M potassium acetate, pH 5.5) was added, mixed by inversion, and incubated on ice for 15 minutes. The mixture was centrifuged at 20,000 x g for 30 minutes at 4°C. The supernatant was removed and recentrifuged at 20,000 x g for 15 minutes at 4°C. A QIAGEN-tip 100 column was equilibrated with 4 ml of a buffer containing 750 mM NaCl, 50 mM MOPS (pH 7.0), 15% isopropanol (v/v), and 0.15% Triton® X-100 (v/v). Supernatant was applied to the equilibrated column and allowed to enter the resin by gravity flow. The column was washed twice with 10 ml of a wash buffer containing 1.0 M NaCl, 50mM MOPS (pH 7.0), and 15% isopropanol (v/v). Elution was done by applying 5 ml of a buffer containing 1.25 M NaCl, 50 mM Tris-HCl (pH 8.5), and 15% isopropanol (v/v). Room-temperature isopropanol (3.5 ml) was added to precipitate the eluted DNA. This was centrifuged at 15,000 x g for 30 minutes at 4°C. The supernatant was removed and the DNA pellet washed with 70% ethanol and centrifuged at 15,000 x g for 10 minutes at 4°C. The supernatant was removed and the pellet was air dried for 10 minutes. Pellets were redissolved in 100-200 μl of nuclease-free H_2O. Concentration and purity was estimated by absorbance readings at 260 nm and 280 nm ([DNA] μg/ml = A_{260} x dilution factor x 50 μg/ml [extinction coefficient]).

Initial sequence of cloned genomic inserts was obtained by dye termination sequencing primed by M13 Forward and Reverse primers with binding sites flanking the

insert. New primers were then designed based on initial sequence results and used to obtain additional sequence (PrimerSelect™; DNASTAR, Inc.). The Virginia Tech DNA Sequencing Facility (Blacksburg, VA) did all sequencing associated with this project (See Appendix C for more detail regarding sequencing).

The "Wild-Type" Construct

Once the sequencing was completed, a "wild-type" expression construct was made. Using cDNAs already isolated encoding the extracellular (Exons 1-13) and transmembrane and intracellular (Exons 14-30) domains, intron 13 was inserted between exons 13 and 14 by means of a three-way ligation (75). The resulting plasmid, referred to as pFIN13, contains the cytomegalovirus intermediate-early promoter plus intron A (40). Additionally, the vector contains a bovine growth hormone polyadenylation site as shown in Figure 5. The FIN13 plasmid has been shown to produce both Flt-1 and sFlt-1 protein and mRNA when incorporated into HEK293 cells (75). The pFIN13 construct serves as the wild type control for analyzing PPy mutants.

Part II: Making the Intermediate Vector and the Mutations

The Intermediate Vector

In order to simplify the introduction of point mutations into the large Flt-1 expression construct (>8 kb insert), an intermediate vector was constructed composed of a fragment of pFIN13 in pLitmus38 shown in Figures 6 and 7. One μg of pFIN13 was digested with 10 units each of *Mlu*I and *Pvu*II in 1x NEBuffer 3 at 37°C for 1 hour. One μg of the pLitmus38 vector was digested with 10 units of *Mlu*I and 20 units of *EcoR*V in 1x NEBuffer 3 supplemented with 100 μg/ml BSA at 37°C for 1 hour. Digests were purified via 1% agarose gel electrophoresis as previously described. The *Mlu*I/*Pvu*II fragment (3180 bp) isolated from pFIN13 was ligated into the *Mlu*I/*EcoR*V-digested pLitmus38 vector. Initially this was transformed into DH5α cells. Colonies were obtained and screened for the *Mlu*I junction (M13Forward/BH206). A positive clone, designated "pL38FMP-b", was streaked and expanded for plasmid DNA preparation. The purified pL38FMP-b was retransformed into the *dam*$^-$ / *dcm*$^-$ *E. coli* strain GM2163

pFIN13 Vector

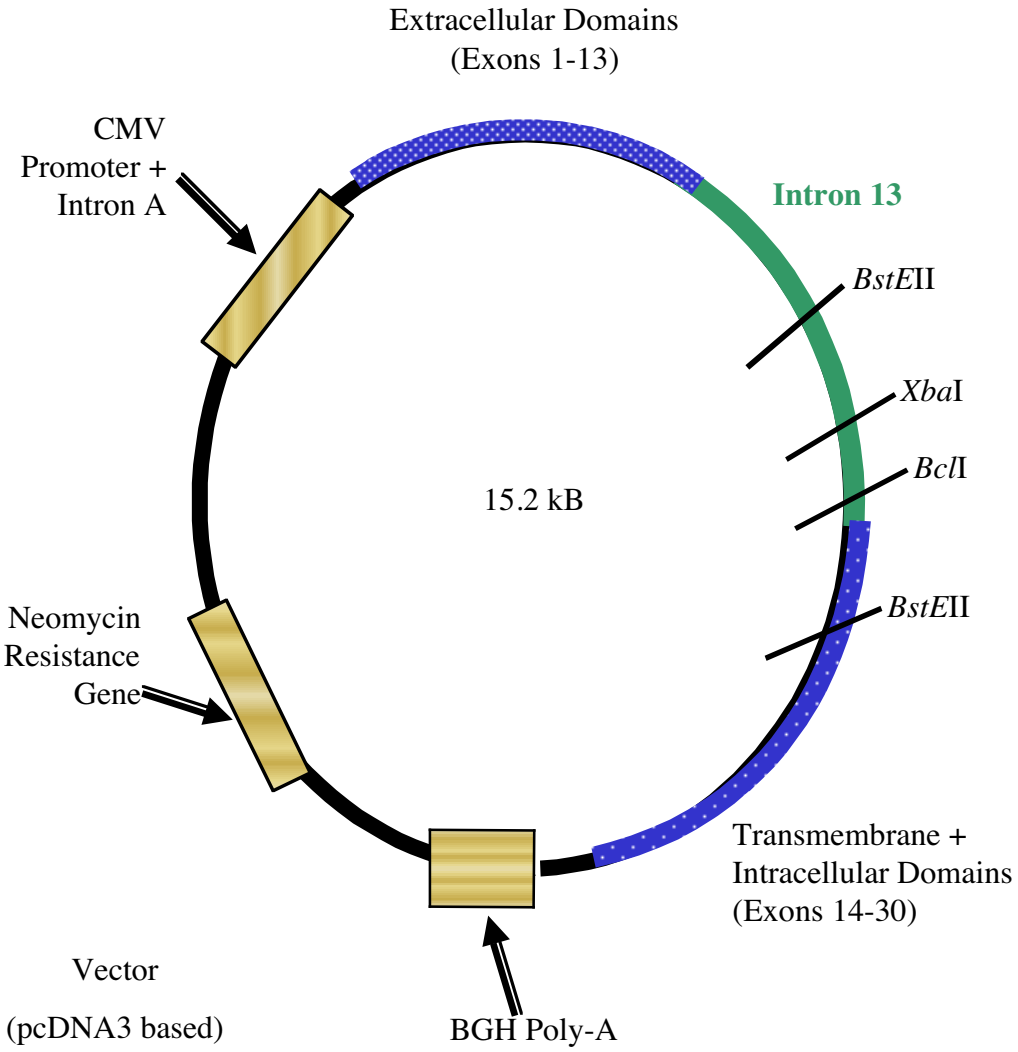

Figure 5. The pFIN13 vector. This vector was transformed into HEK293 cells once a mutation was incorporated. Restriction site locations are shown. CMV= cytomeglo virus. BGH=bovine growth hormone. (Figure not to scale).

Intermediate Vector

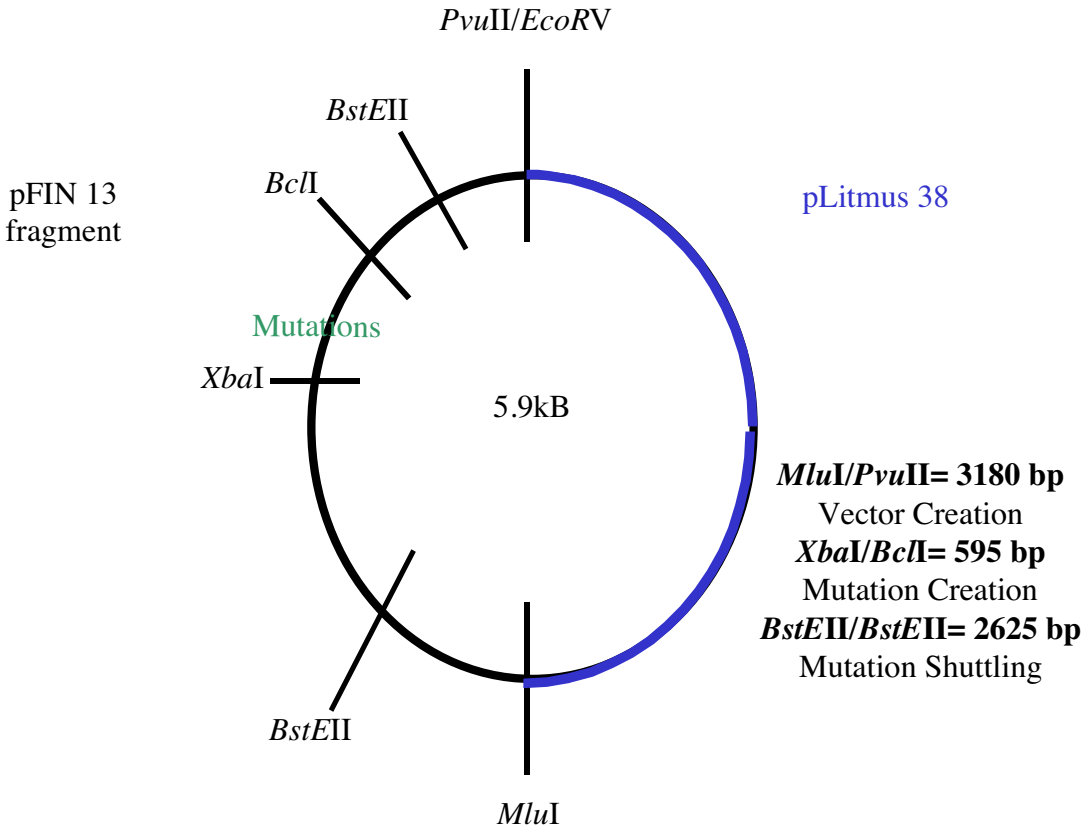

Figure 6. The Intermediate vector structure used for creating mutations. The primary advantage was the ability to sequence only a small portion of the final product (XbaI-BclII) for mutation conformation. (Figure not to scale).

Linearized Vector Structure

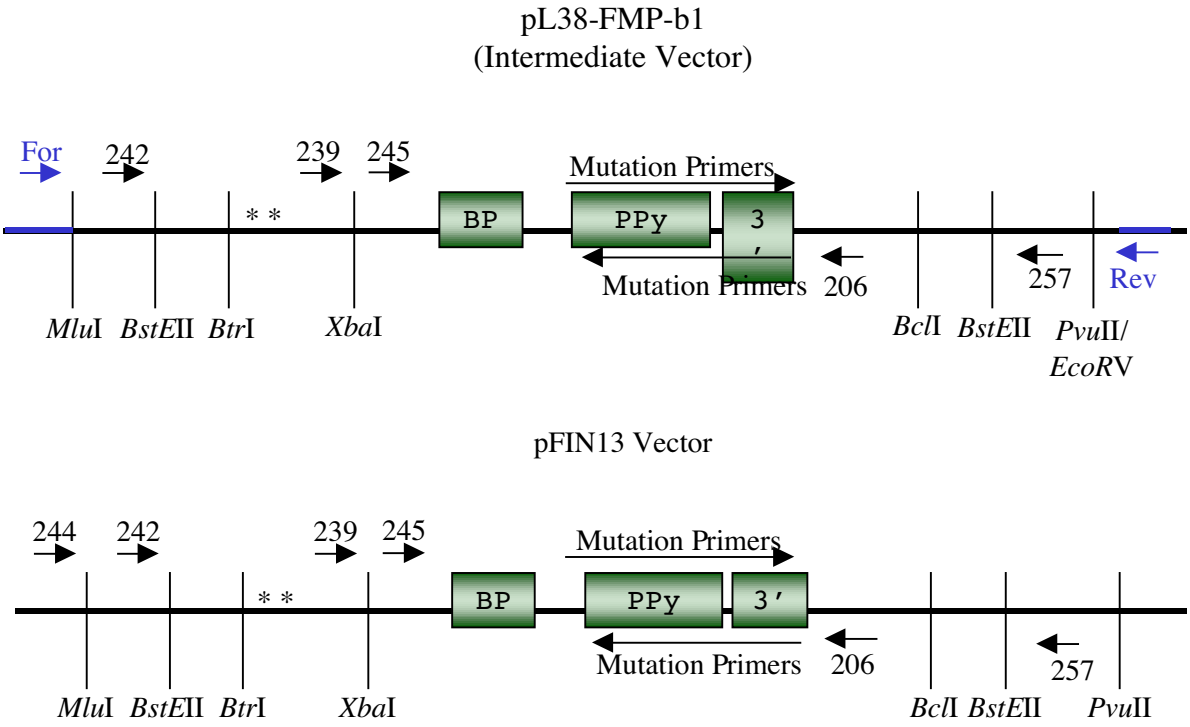

Figure 7. Linearized Vector Structure. Portions of the two vectors are presented in linear form for ease of visualization. Utilized restriction endonuclease sites are shown. Primers used either for sequencing or creating are also shown. * denotes two of the polyadenylation sites. (Figure not to scale).

cells (as previously described for DH5α cells; see Appendix D for GM2163 competency protocol). Colonies were screened as above. Positive clone "pL38FMP-b1" was streaked and expanded in 100 ml LB-amp plus 12.5 μg/ml chloramphenicol for plasmid preparation.

Mutation Design and Creation

Primers were designed to create mutations in the PPy tract (PrimerSelect™; DNASTAR, Inc.). Table 1 shows primer alignment to intron 13 sequence and designated mutations. Mutations were made by adapting a PCR-based protocol designed for creating chimeras (74) (Figure 8). Two rounds of PCR were done using the same conditions (Appendix E, Program 2). The first round created two arms (about 480 and 1680 bp) that were then used as the templates in the second round to create the faux chimera. Reaction conditions for round 1 consisted of either: i) 1.25 units *Pfu* polymerase, 1x buffer (Stratagene®), 0.4 mM dNTP's, 1 μM of each primer, 100 ng of template (pFIN13) and DNase/RNase free water taking the volume to 20 μl, or ii) 1x QIAGEN *Taq* PCR Master Mix, 1 μM of each primer, 100 ng of template (pFIN13) and DNase/RNase free water to bring the volume to 20 μl. Round 1 products were purified via 1% agarose gel electrophoresis. Round 2 PCR reactions consisted of 1x *Taq* PCR Master Mix, 1 μM of each primer (BH239/BH257), 100 ng template (~1 μl of the 20 ul purified PCR products from Round 1) and DNase/RNase free water to bring the volume to 20 μl. After each round of PCR, the products were fractionated using 1% agarose gel electrophoresis and purified.

Purified round 2 PCR products (0.5 – 1 μg) were digested with 15 units of *Bcl*I in NEBuffer 3 plus BSA at 50°C for 1 hour, followed by the addition of 20 units of *Xba*I and further incubation at 37°C for a second hour. Simultaneously, pL38FMP-b1 was digested the same way. The digested vector was purified using 1% agarose gel electrophoresis. Digested PCR products were purified via 2% agarose gel electrophoresis. Ligation mixtures included approximately 100ng of each insert and vector. A vector-only null ligation was also included to determine the level of background. Each ligation reaction was transformed into DH5α cells. Recombinant

Table 1. Identification of Mutations and Primers

Mut. Name	Mut # in IV**	Mut # pFIN13	Primer #	Primer Sequence and Direction*	Expected Splicing Change
Wild Type††	-	5	–	CCACACCCCCTCTCTTTCCTCGCTAGATT	N/A
G/A Mut†	-	2	258	CACGCACGCACGTACGTCGCTAGATTCGG →	–
			259	ATATTTATTGGTGTGCGTGCGTGCATGCAG ←	
Flip/ Flop	D2	51	281	ACATTTTTCTCTCCCTTCTGCTAGATTCGG →	+
			282	TTATATTTATTGGTGTAAAAAGAGAGGGAA ←	
C/T Alt	A1	512	283	AACCACACTCTCTCTCTCTCTCTGCTAGAT →	?
			284	TTGGTGTGAGAGAGAGAGAGAGACGATCTA ←	
All C	E2	511	285	ACCACACCCCCCCCCCCCCCGCTAGATT →	–
			286	TGGTGTGGGGGGGGGGGGGGCGATCTAA ←	
T to G	E2	55	287	CCACACCCCCGCGCGGGCCGCGCTAGATTC →	–
			288	GGTGTGGGGGCGCGCCCGGCGCGATCTAAG ←	
5T	B2	59	289	CACCCCCTCTTTTTCCTCGCTAGATTCGG →	+
			290	GTGGGGGAGAAAAAGGAGCGATCTAAGCC ←	

** IV designates the intermediate vector.

* The boxed area designates the location of the polypyrimidine tract in relation to the primer. Mutated bases are blue.

†† Sequence designated with Wild Type is original sequence of the polypyrimidine tract without any changes.

† G/A Mut was created before use of the IV was implemented.

Mutation Creation Protocol

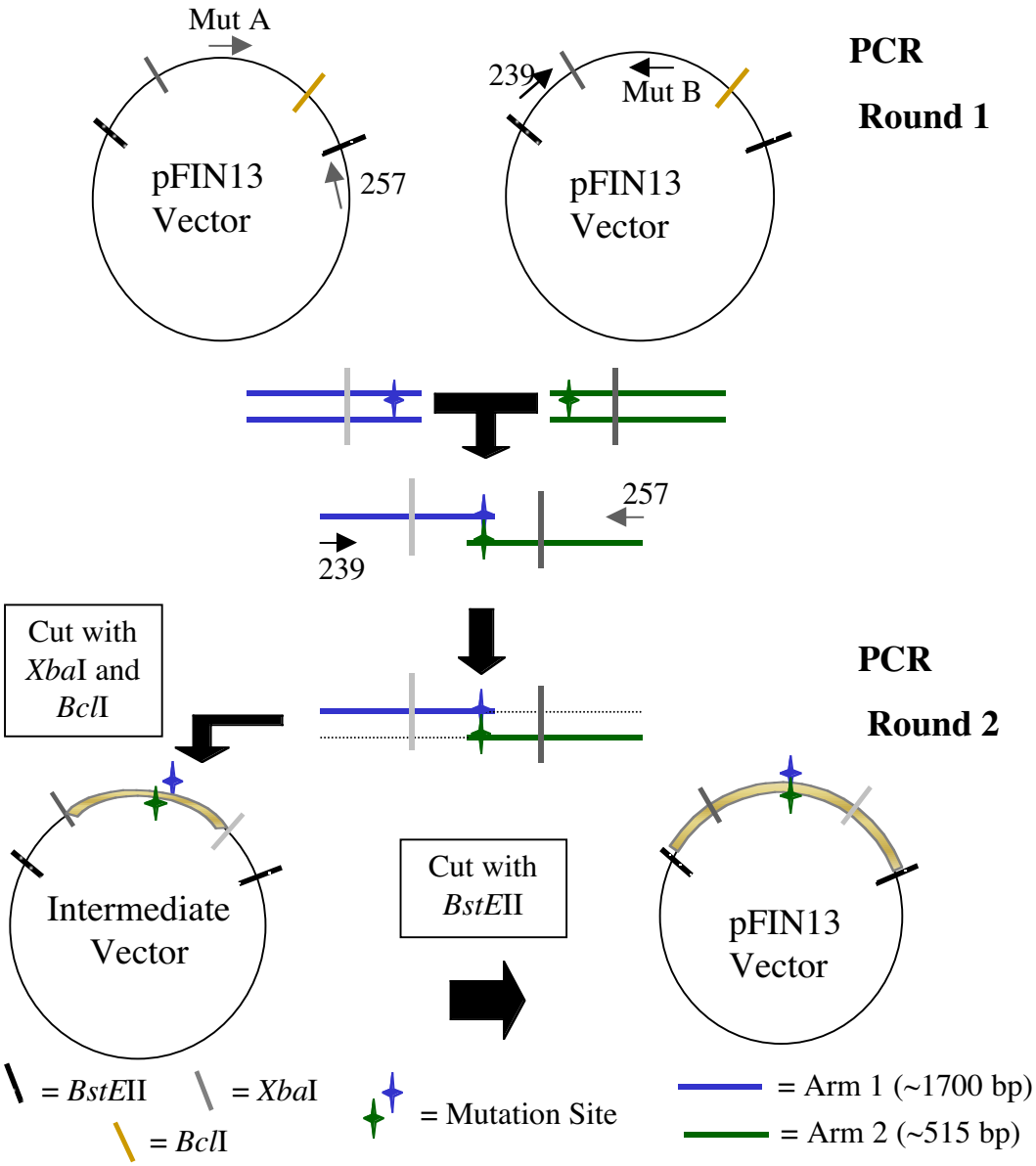

Figure 8. Creating the mutations. Using pFIN13 as a template, 2 separate PCR reactions were set up using a primer containg a one set of mutations and an outside primer either 257 or 239 as shown. These are purified using agarose gel electorphoresis. These purified PCR products are then used as templates in the second round of PCR. One reaction is set up with both first round products as the template and 257 and 239 as primers. This is again purified using gel electrophoresis. The second reound PCR product is then digested using *Xba*I and *Bcl*I and ligated into the Intermediate Vector (IV) previously cut with *Xba*I and *Bcl*I. IV is cultured, screened by sequencing, and purified. The IV, containing the mutations, and pFIN13 vectors are digested with *BstE*II and CIP treated to facilitate moving the mutated region into pFIN13.

colonies were screened with PCR using BH239/BH206 that flank the *Xba*I/*Bc*lI insert fragment. PCR products (~600 bp) were purified on 2% agarose gel electrophoresis and sequenced with BH245 to confirm the presence of the desired mutations. The mutated pL38FMP-b1 clones were streaked and expanded for plasmid preparation. Mutated intermediate vectors were digested with 10 units of *BstE*II with 1x NEBuffer 3 plus BSA at 60^{o}C for 1 hour, followed by 20 units of *Dra*III and further incubation at 37^{o}C for 1 hour. Simultaneously, pFIN13 was digested with *BstE*II, followed by CIP treatment for 1 hour at 37^{o}C. The gel-purified, mutated 2630 bp *BstE*II fragments were ligated to the gel purified *BstE*II digested pFIN13 vector and transformed into DH5α cells (as described previously). Vector-only null ligation mixture was also set up to determine background. Recombinant colonies were screened with PCR for the *BstE*II junction occurring in intron 13 and proper insert orientation (BH244/BH206). Positive clones were streaked and expanded, and purified plasmid was sequenced again with BH245 for mutation confirmation.

Part III: Testing the Mutations

The effects of PPy mutations on Flt-1 and sFlt-1 expression were tested as outlined in Figure 9. Appendix C contains information regarding cell culture reagents.

Transfecting HEK293 Cells

Once these mutations were made and confirmed by DNA sequencing, the plasmids were transfected into HEK293 cells using a liposomal formulation (Mirus TransIT®-293). Stock T75 flasks of HEK293 cells (ATCC) maintained in Dulbecco's Modified Eagle Medium/10% Fetal Bovine Serum/50 μg/ml Gentamycin (DMEM/FBS/Gent) were washed once with 10 ml of Dulbecco's Phosphate Buffered Saline without Ca^{2+} or Mg^{2+} (DPBS). Cells were harvested with 2 ml of DPBS containing 0.5 mg/ml Trypsin plus 0.2 mg/ml Na_4EDTA for 10-15 minutes at room temperature. Trypsin was inactivated by the addition of 8 ml of DMEM/FBS/Gent, and cells were counted on a hemocytometer with Trypan Blue staining (0.2% final). Individual 60 mm dishes (Corning) containing 6 x 10^5 HEK293 cells in 5mls

Part II. Experimental Design

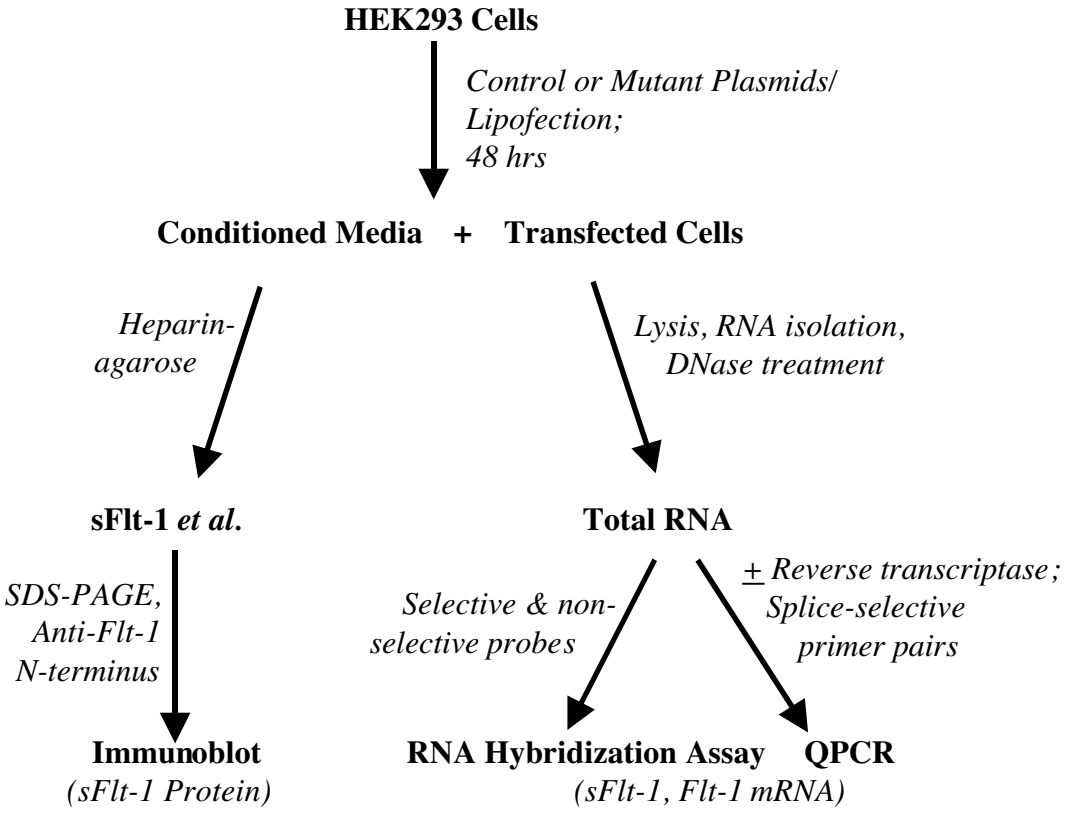

Figure 9. Once each mutation was made and confirmed by sequencing, it was transiently transfected into HEK293 cells via lipofection. After 48 hours, the media and cells were harvested and used for western blotting, northern blotting or quantitative PCR. Three independent experimental replicates were done.

DMEM/FBS/Gent were prepared and allowed to incubate at 37°C (5% CO_2). When cells became 50-70% confluent (typically overnight), the medium was replaced and the cells returned to the incubator for 30 minutes. Two hundred and fifty μl of OptiMEM-I (Life Technologies™) and 9 μl of TransIT-293 were mixed in a sterile polypropylene tube and incubated at room temperature for 10 minutes. Three μg of plasmid DNA was added to this mixture and again incubated for 10 minutes at room temperature. This liposome/DNA mixture was then added dropwise to each dish (~10^6 cells) while swirling. The dishes were then swirled again to distribute the mixture evenly and returned to the incubator for 48 hours.

Harvesting of Media

Each dish of transfected cells was handled individually. Media were removed and cells were harvested from one dish prior to removing a second from the incubator. Medium was collected from each dish of cells into a 15-ml conical bottom tube and centrifuged for 5 minutes at 150 x g to remove cells and debris. Supernatant was removed to a clean 15-ml tube. Once all dishes of cells have been handled, the media could then proceed to the next stage of treatment. A suspension of heparin-agarose beads (Sigma®) was washed 2 times with 10 volumes of ddH_2O and centrifuged for 5 minutes at 150 x g. The supernatant was aspirated, and ddH_2O was added 1:1 to the bead pellet. This mixture was aliquoted to each tube of conditioned media supernatant (160 μl suspension/tube). The media were then incubated overnight at 4°C with end-to-end mixing. The tubes were then centrifuged at 260 x g for 10 minutes. Supernatants were aspirated and the beads were washed with 1 ml DPBS, transferred to 1.5-ml microcentrifuge tubes, and centrifuged at 14,000 x g. Supernatants were aspirated and the 15-ml tubes were rinsed with 1ml DPBS that was transferred to the pelleted heparin beads in the 1.5-ml tube. The 1.5-ml microcentrifuge tubes were centrifuged at 14,000 x g and the wash was repeated 1 more time. The pelleted beads were resuspended with an equal volume of 2x Laemmli Sample Buffer (Sigma®) and stored at –20°C.

Harvesting of Cells

Cells were harvested after removal of the medium from each dish and washing with 5 ml DPBS. Six hundred μl of buffer RLT (containing guanidine thiocyanate [QIAGEN]) plus 1% β-mercaptoethanol was added to the dish. A plastic cell lifter (Costar®) was used to scrape the cells off the dish surface. Cell lysate was then transferred to a centrifugal homogenizer (QIAshredder, QIAGEN). Once all dishes were handled, QIAshredders were centrifuged at 14,000 x g for 2 minutes. Homogenized lysates were then stored at –20°C.

RNA Isolation and cDNA Synthesis

RNA was isolated from the homogenized lysates using a silica-gel-based membrane technique (RNeasy® Mini Kit, QIAGEN) including treatment with 30 units of RNase-Free DNase (QIAGEN). Samples were eluted from membranes with two applications of 40 μl of nuclease-free water. Estimated sample concentrations and purity were approximated using absorbance readings done at 260 nm and 280 nm ([RNA] μg/ml = A_{260} x dilution factor x 40 μg/ml [extinction coefficient]). Total RNAs were stored at –20°C, short term. cDNA was then synthesized using random primers and MMLV-Reverse Transcriptase (RETROscript™, Ambion®). Two μg of sample and random decamers (100 pmol) were used with heat denaturation of the RNA in the first step of the protocol. Complete reactions were set up with reverse transcriptase (RT), and the protocol was stopped after the RT was heat-inactivated; separate samples were prepared containing 2 μg total RNA without RT. All reactions were then diluted to 50 μl (40 ng RNA equivalent/μl) and stored at –20°C for later use.

Real-Time Quantitative Polymerase Chain Reaction (QPCR)

Prior to running this experiment, a target dilution curve was developed for each target (Flt-1, sFlt-1, and neo^r mRNAs), confirming that efficiencies were comparable for each target (75). Each QPCR reaction contained 12 ng of cDNA (RNA equivalents) or non-reverse transcribed total RNA, 1x buffer A (PE Biosystems), 3.5 mM $MgCl_2$, 0.2 mM of each dNTP, 0.025 units/μl of AmpliTaq Gold, 0.01 units/μl of AmpErase UNG,

0.3 μM of each primer and 0.2 μM of the probe. Six sets of reactions were set up: two sFlt-1 (BH211/BH212, TP1 probe, cDNA and no RT), two Flt-1 (BH228/BH229, TP3 probe, cDNA and no RT), and two neo^r (BH296/BH297, TP5 probe, cDNA and no RT). Figure 10 shows primer and probe binding locations for the three targets. Appendix 1 shows primer and probe sequences. Each reaction mix was distributed into 3 optical PCR tubes (Perkin-Elmer) and put into the ABI Prism® Sequence Detection System (SDS) 7700 plate. Reactions were run under the following conditions: stage 1, 50°C, 2 minutes; stage 2, 95°C, 10 minutes; stage 3, 95°C, 15 seconds, 60°C, 1 minute, 40 cycles.

A randomized complete block design was used in this experiment. Blocks were established across time and each mutation is a treatment. A mixed effect analysis of variance (ANOVA) was used for data analysis on ΔΔCt values. Block was treated as a random effect. Treatment was a fixed effect.

RNA Hybridization Assay

Probes were designed and created using restriction endonuclease digestion of pPCRSprint–T216217 (digested with 20 units of *Pst*I and 10 units of *Not*I in NEBuffer 3 supplemented with BSA at 37°C for 1 hour) for the Flt-1 probe, pPCRSprint–T201202 (digested with 20 units of *Sac*I and *Xho*I in NEBuffer 3 supplemented with BSA) for the probe that detects both Flt-1 and sFlt-1 mRNAs, and pL38–E3.3ΔBsrGI (digested with 20 units of *Sma*I in NEBuffer 4 at 25°C for 1 hour, followed by the addition of 20 units of *Hind*III and subsequent incubation at 37°C for 1 additional hour) for the sFlt-1 probe. Each probe was purified using 1% agarose gel electrophoresis. Each was then labeled using BrightStar™ Psoralin-Biotin Nonisotopic Labeling Kit (Ambion®). Probe binding locations are shown in Figure 11.

The RNA hybridization assays were all run using NorthernMax™ Protocol and Kit (Ambion®). Five μg of each sample was mixed with the loading buffer (1:3 by volume) and EtBr (10 μg/ml final concentration) and loaded onto a 1% agarose denaturing gel containing formaldehyde. When RNA samples were too dilute (<0.75 μg/μl), aliquots containing 5 μg were dried in a RapidVap (Labconco) until no fluid remained in the tubes (~2-3 hours) to concentrate the samples. Each sample was then

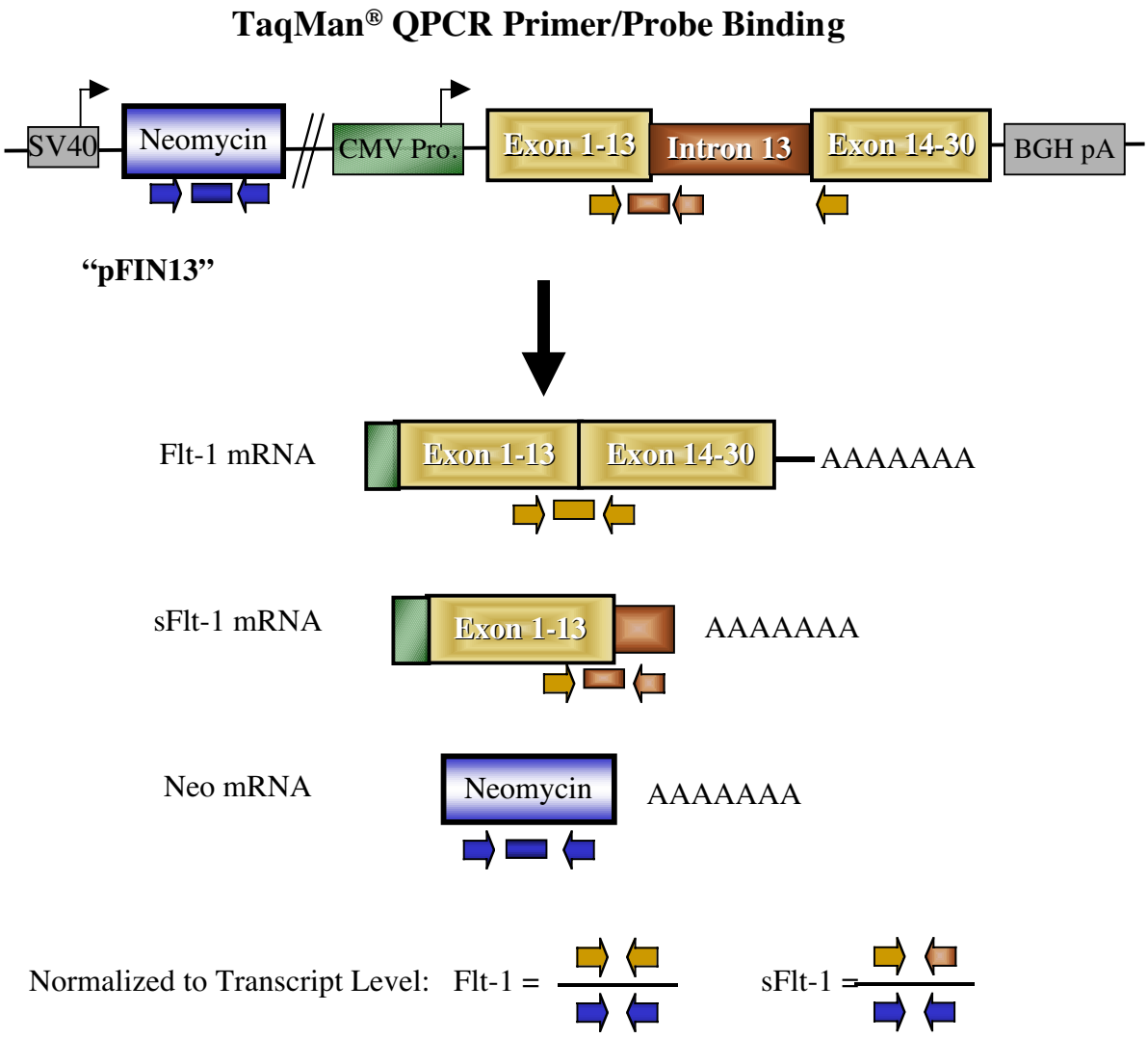

Figure 10. Location of the TaqMan® primers and probe for each of the QPCR targets. Note the ability of the sFlt-1 target primers/probe to bind to plasmid DNA as well as mRNA-derived cDNA. For each sample run, a "no RT" was included. This allowed us to remove background signal contributed by plasmid carryover. The neo^r target was used as a way to normalize Flt-1 and sFlt-1 expression levels. QPCR used the ABI SDS 7700.

RNA Hybridization Assay Probe Binding Sites

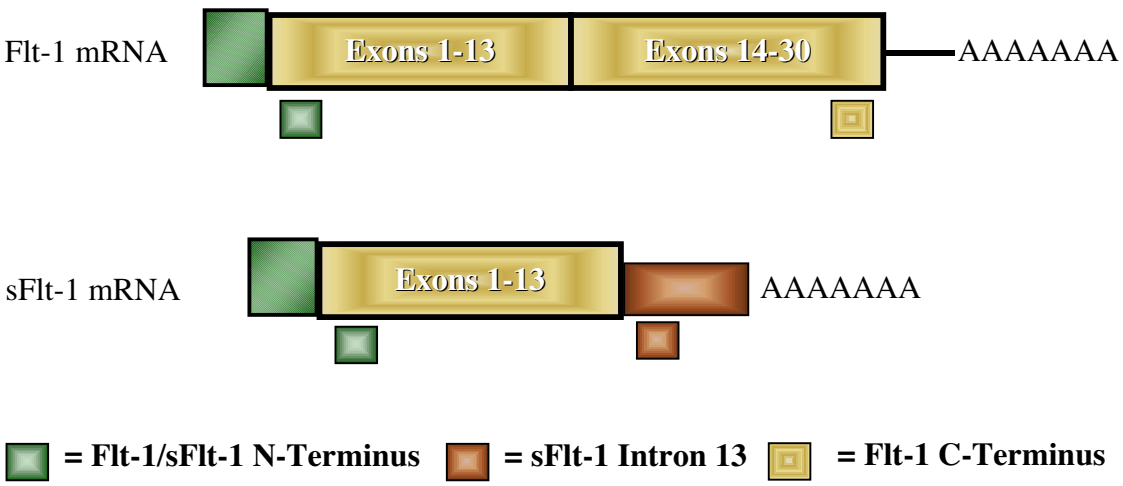

Figure 11. RNA hybridization assay probe binding locations. Three restriction digest fragments were nonisotopically labeled using Ambion's BrightStar™ Psoralen-Biotin Kit, and then used as probes for northern blots done with Ambion's NorthernMax™ Kit.

reconstituted in 5 μl of DNase/RNase free water and 15 μl of loading dye and EtBr (as designated above) before being loaded on the gel. BrightStar™ Biotinylated RNA Millennium™ Markers (Ambion®) were used according to the vendor's recommendations (one lane per gel). The transfer step was done with an upward transfer apparatus as indicated below and transferred overnight. The gel casting tray was inverted in 9"x9" Pyrex® dish with ~500 ml alkaline (10 mM NaOH) Transfer Buffer provided by Ambion® or 20x Saline-Sodium Citrate (SSC). The rest of the stack was formed as follows: wick (2 pieces of Whatman 3MM chromatography paper set end to end), 3 pieces of Whatman 3MM chromatography filter paper (pre-wet in transfer buffer), gel, guard (Parafilm®), membrane (Zeta-Probe® GT Genomic Tested Blotting Membranes, BioRad, pre-wet in transfer buffer), 2 more pieces of 3MM paper (dry), paper towel stack (dry), weight (150-200 g). When 20x SSC buffer was used as the transfer buffer, gels were washed in 50 mM NaOH for 20 minutes to fragment RNAs and then in 20x SSC for 45 minutes to re-equilibrate for transfer. Crosslinking of RNA to the membrane was done in a Stratalinker® UV Crosslinker (Stratagene® Model 1800) on the autocrosslink mode (~25-50 seconds).

Hybridization, using ~1 pM of probe, proceeded for 4 hours in a formamide-containing buffer (ULTRA-hyb™, Ambion®). Detection was done using the BrightStar™ BioDetect™ Nonisotopic Detection Kit and Protocol (Ambion®). Membranes were exposed to X-ray film (Kodak, BIOMAX™ML) for a duration of 0.5, 2, 6,10, 20 or 30 minutes as needed. Upon completion of detection with one probe, the membranes were stripped (0.1% sodium dodecyl sulfate [SDS] in diethyl pyrocarbonate [DEPC]-treated water brought to boiling, poured over the membrane and allowed to cool to room temperature) and reprobed. Membranes were held at room temperature between two pieces of 3MM paper and paper towels for long term storage. Each exposure was scanned into a computer using a VXR-12 film digitizer (Vidar Systems Corporation), and densitometric analysis was performed on a Power Macintosh G3 computer using the public domain NIH Image program version 1.62 (developed at the U.S. National Institutes of Health and available on the Internet at http://rsb.info.nih.gov/nih-image/).

A randomized complete block design was used in this experiment. Blocks were established across time and each mutation is a treatment. Rank-transformed data was utilized to stabilize the variance. A mixed effect ANOVA was used for data analysis. Block was treated as a random effect. Treatment was a fixed effect. Tukey's HSD was used to compare treatments. For ease of understanding, the means of the raw data are presented in addition to the mean ranks.

Protein Immunoblotting

Heparin-agarose-adsorbed conditioned media collected from transfected HEK 293 cells were used in the protein immunoblots. Washed bead pellets in Laemmli sample buffer (see above) were heated for 5 minutes at 95^{o}C and centrifuged at 14,000 x g for 2 minutes. Twenty five μl were loaded into precast 8-16% SDS-polyacrylamide gels (9x10 cm; PAGEr™ Gold Precast Gells, BMA); prestained SDS high-range markers (BioRad) were also loaded. The gels were run at 125 V for approximately 45 minutes until the dye front reached approximately 2 cm from the bottom. Once completed, the transfer apparatus was set up in a small container of 1x transfer buffer (0.25 M Tris base, 1.92 M glycine and 10% MeOH) as follows: cartridge, sponge, filter paper, membrane (Immobilon^{TM}–P Transfer Membrane), gel, filter paper, sponge and the other half of the cartridge. All air bubbles were removed between each layer by rolling a test tube over the submerged materials. This "sandwich" was then placed into the transfer box, and the box filled with transfer buffer. The transfer was run for 60 minutes at 100 V (amps<0.35) with the cooling unit in place. During this time, blocking buffer (0.2% gelatin in TNT [25 mM Tris-HCl, pH 7.5, 150 mM sodium chloride, and 0.02% Tween-20]) was made and heated to dissolve the gelatin. Once completed, the apparatus was disassembled and the membrane washed in 1x TNT for 5 minutes. The membrane was transferred to blocking buffer and allowed to shake overnight at 4^{o}C. The membrane was then rinsed again with 1x TNT for 5 minutes. The membrane was then transferred to a clean container and incubated at room temperature for approximately 1 hour with 0.2 μg/ml primary antibody (anti-Flt-1 N-terminus; Santa Cruz, sc-9029) in blocking buffer. Upon completion, the membrane was washed 4 times at 5 minutes each in 1x TNT with shaking

at room temperature. Secondary antibody (Horseradish peroxidase-conjugated goat anti-rabbit IgG; Southern Biotechnology Associates, 1:10,000 in blocking buffer) was then added to the membrane and incubated at room temperature with shaking for approximately 1 hour. The membrane was then washed 4 times at 5 minutes each in 1x TNT with shaking at room temperature. Detection reagents (SuperSignal® West Pico Chemiluminescent Substrate, Pierce) were then added to the membrane and incubated for 5 minutes at room temperature. The excess fluid was allowed to drip off and the membrane was wrapped in plastic wrap prior to X-ray film exposure (Kodak, BIOMAX™ML) for 10 seconds, 40 seconds, and 2 minutes. Each exposure was scanned and subjected to densitometric analysis as described for the RNA hybridization films presented above.

A randomized complete block design was used in this experiment. Blocks were established across time and each mutation is a treatment. A mixed effect ANOVA was used for data analysis. Block was treated as a random effect. Treatment was a fixed effect. Tukey's HSD was used to compare treatments. This data was not rank-transformed.

RESULTS

The objective of this project was to determine if changes in the splicing signals of Flt-1 intron 13 would result in changes in expression (mRNA and protein) of sFlt-1. We approached this objective by making mutations, transfecting cells and testing harvested cells and conditioned media with QPCR, protein immunoblotting, and RNA hybridization assays. Prior to doing this, however, structural information was obtained about intron 13. Intron 13 was sequenced on both strands by the dye termination sequencing method (Appendix C). The strength of the splicing sites within intron 13 was then predicted by comparison to published consensus sequences (Figure 4). Splice sites at the 5' and 3' ends of Flt-1 intron 13 match the two-base sequences of a U2-dependent intron (GU/AG) (47, 54, 72). Intron 13 has a potential branch point sequence that also matches the consensus sequence (CUGAU) (75). However, the consensus for the branch point is much more liberal than the 5' and 3' splice sites. In fact, using mutational analysis, it was determined that if alterations in the wild type branch point rendered it inactive, cryptic sites could be utilized that had little or no similarity to the consensus including use of a cytidine or uridine if no adenosine residue was present (52). Therefore, mutations to the branch point were not made. However, the PPy tract does not have a strict consensus, but trends do exist for its strength. Typically, the longer the tract, the more efficiently it functions. Also, if the tract contains more uridine residues, it should have improved functions. In the case of intron 13, the PPy tract is of an intermediate length (16 nucleotides) but is relatively low in uridine (10:6, C:U). Due to the low uridine content, in addition to a deficiency in consecutive uridines, it was decided that alterations in the content of the PPy tract would be made. It was postulated that changing the composition of the PPy tract would increase or decrease the strength of the tract as a splicing signal for Flt-1 mRNA production; consequently, sFlt-1 mRNA production might be altered by changing the availability of pre-mRNA.

Mutational Design and Creation

Mutational analyses of PPy tracts have demonstrated that, in a moderate-length tract, substitutions of purines for uridine residues caused a marked decrease in

spliceosome formation and splicing product. Conversely, an increase in uridine content was shown to improve splicing efficiency. Based on this information, a set of base changes was selected and created in the PPy tract of intron 13 (Table 1). Three of these mutations were predicted to enhance splicing while the other three were expected to worsen splicing.

A PCR-based mutational strategy was selected to create the mutations (Figure 8). Each primer was designed to contain the desired base changes. Using these and two non-mutated "outside" or flanking primers, two reactions were set up (one mutated primer and one outside primer per reaction) with pFIN13 as the template for each desired mutation. The products from these reactions were fractionated, purified and used as the templates in round 2 with the two flanking primers. These products, containing the desired mutations, were purified and digested with *Xba*I and *Bcl*I. The mutation-containing fragments (595bp) were ligated into the intermediate vector for ease of handling and to minimize the size of PCR-amplified segments that would need to be sequenced and transferred back to pFIN13 (Figure 5 and 6). When the intermediate vectors containing the mutants were being assembled, a problem arose. Test digests were done to prepare the vector for the ligation of the insert. The restriction enzyme *Bcl*I did not cut the vector. DNA methylation, which can interfere with *Bcl*I-catalyzed DNA cleavage, was suspected to be the cause of the problem. To overcome this, the non-mutated intermediate vector was transformed into a *dam*$^-$, *dcm*$^-$ strain of *E. Coli* (GM2163) that does not methylate DNA. The intermediate vector DNA derived from the GM2163 transformants was cut efficiently by *Bcl*I and was used as a recipient for mutated inserts.

Initially, *Pfu*, a proofreading, thermostable polymerase, was used in mutant preparation to reduce the likelihood of PCR-induced artifacts. However, *Taq* polymerase provided superior amplification efficiency and was used as the primary polymerase in these reactions. Upon completion of sequence confirmation, each mutation was moved into pFIN13. (Note: The G/A mutation was created by using flanking primers that anneal outside of the *BstE*II sites in pFIN13. The mutant containing fragment was shuttled directly back into pFIN13, skipping the intermediate vector step.) The use of *Taq* polymerase had an unexpected consequence in the preparation of the "Flip-flop" (primers

BH281/BH282) mutant. *Taq* polymerase appends an adenosine residue to the 3' ends of double stranded PCR products. As a result of this, an additional C to T change was created four bases upstream of the PPy tract in the "Flip-flop" mutant (Table 1). Rather than correcting this change (for example by using *Pfu* polymerase), we elected to utilize it as an extended mutant. The final product obtained from this portion of the project was 11 constructs, 5 mutations in the intermediate vector and 6 in pFIN13.

Analysis of Mutations

Cell Transfection and Harvesting

The next step in the project was to transiently transfect HEK293 cells with the mutated pFIN13 plasmids to determine effects of mutations on sFlt-1 and Flt-1 expression (Figure 9). HEK293 cells were chosen because they are a readily-transfectable, non-endothelial cell type. Expression of VEGF receptors is not typically detectable in these cells, so signals observed from the cells is likely to be a consequence of transfection. The Flt-1 sequences used in this project are murine in origin, so any endogenous expression or genomic DNA contamination from the human cell line can be excluded by the highly specific QPCR analysis and not contribute background (Figure 12). The cells were transiently transfected via a lipofection method. After 48 hours, both the conditioned media and cells were harvested. The conditioned media were heparin-agarose treated to partially purify sFlt-1 protein, and run on protein immunoblots. The cells were lysed and RNA isolated. A DNase treatment was included to reduce background caused by transfected plasmid that may be present in the isolated in the RNA. A fraction of total RNA was reverse-transcribed to make cDNA. The cDNA could then be used in the QPCR assay. Another portion of the total RNA was used in the RNA hybridization assay. This process was done for all three independent experiments run (Rep 1, 2, and 3). The following sections provide results obtained from each of these tests in more detail.

Human/Murine Sequence Comparison

MOUSE and HUMAN sFlt-1 (exon 13/intron 13 junction)
QPCR Primers (BH211/212) and Probe (TP-1)

MOUSE and HUMAN Flt-1 (exon 13/14 junction)
QPCR Primers (BH228/229) and Probe (TP-3)

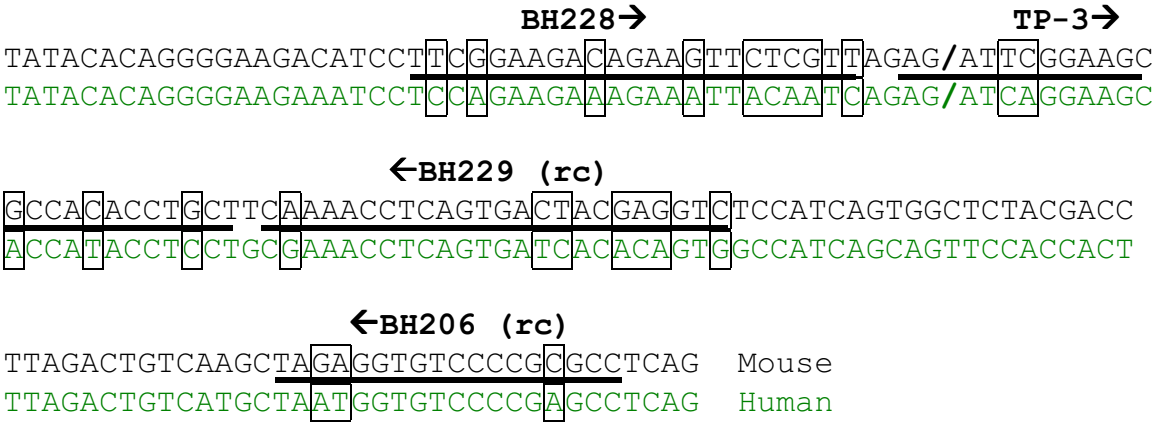

Figure 12: Homology between Human and Mouse sFlt-1 and Flt-1 sequence at the location of the QPCR primers and probes. Boxed bases differ between species. Underscore denotes primer or probe. BH206 is shown as a reference.

Quantitative PCR

QPCR was chosen because of its high level of specificity. We wanted to know, specifically, if Flt-1 mRNA levels and sFlt-1 mRNA levels changed with respect to an internal control (neo^r mRNA). For three different targets (Flt-1, sFlt-1 and neo^r), triplicate reactions were set up and run in the ABI Prism® Sequence Detection System (SDS) 7700. Figure 10 presents primer and probe binding locations. Primer and probe sequences are presented in Appendix A. For the three targets, a "no RT" control was set up and run in triplicate as well. This set of reactions provided a way to correct for any background due to the presence of plasmid DNA that could contribute to the neo^r and sFlt-1 signals. In addition to removing plasmid background, internal normalization was done to allow comparisons to be made between sFlt-1 and Flt-1. The neo^r target serves as normalization for the other two targets. It is expressed under a separate promoter present in the FIN13 plasmid. Because this is internal to the plasmid, it eliminates variation due to transfection, handling, and reaction efficiency. The ABI software determines a threshold cycle (Ct) at which a product is measurable over noise. The smaller this number the fewer cycles it takes to detect a signal and therefore the more target is present in the reaction. Flt-1 and sFlt-1 mRNA expression levels (normalized internally to neo^r mRNA) relative to levels in wild-type transfectants were calculated by the "ΔΔCt" method. The ΔCt is the difference between Flt-1 (or sFlt-1) Ct and neo^r Ct for a given sample (corrected for plasmid background). The ΔΔCt is the difference between ΔCts for a given sample and that occurring in the wild-type. Ratios to wild-type are then calculated as $2^{-\Delta\Delta Ct}$ to account for a two-fold difference in target concentration per cycle. With this method, differences in how sFlt-1 and Flt-1 change can be detected in addition to how the Flt-1: sFlt-1 ratio changes.

Table 2 presents data obtained from this experiment. Mutations G/A Mut, All C, and T to G, all of which reduced the uridine content of the PPy tract, had a decreased level of expression of Flt-1 mRNA. The 5T, C/T Alt mutants, which increased uridine content, and the polyadenylation mutant (ΔpA1-6) had an increased level of Flt-1 expression relative to the wild-type. The Flip-flop mutant, although it also increased uridine content, showed only a small increase in Flt-1 mRNA expression, and no relative

Table 2. QPCR Results

Table 2. QPCR results. The ABI software determines a threshold cycle (Ct) at which a product is measurable over noise. The smaller this number the fewer cycles it takes to detect a signal and therefore the more target is present in the reaction. Flt-1 and sFlt-1 mRNA expression levels (normalized internally to neo mRNA) relative to levels in wild type (WT, #5) transfectants were calculated by the "ΔΔCt" method. ΔCt is the difference between Flt-1 (or sFlt-1) Ct and neo Ct for a given sample. ΔΔCt is the difference between ΔCts for a given sample and the WT. Ratios to WT are then calculated as $2^{-\Delta\Delta Ct}$ to account for a 2-fold difference in concentration per cycle. ΔpA 1-6 (#17) is a mutant defective in sFlt-1 mRNA poly-adenylation. The mean and standard deviation (StDev) are presented for the three independent experiments. Statistical analysis was done on relative thereshold values.

Mutation		Mean across Reps	StDev across Reps		Mean across Reps	StDev across Reps	
Name	No.	Flt:neo			sFlt:neo		
WT	5	1.00	0.00	-	1.00	0.00	-
T to G	5 5	0.0029	0.0012	*	1.67	0.57	
G/A	2	0.0083	0.0022	*	1.68	0.56	*
All C	5 1 1	0.47	0.29	*	1.66	0.80	
Flip/Flop	5 1	1.22	0.18		0.92	0.42	
5T	5 9	1.94	0.89	*	1.13	0.38	
C/T Alt	5 1 2	2.03	0.36	*	0.83	0.25	
ΔpA1-6	1 7	5.70	0.72	*	0.20	0.10	*

change in sFlt-1 mRNA. Irrespective of the range of Flt-1 mRNA expression, sFlt-1 expression was not dramatically affected by the PPy mutations. G/A Mut and ΔpA1-6 are the only mutations that show relative changes in sFlt-1 expression. The ΔpA1-6 was intentionally created to be severely defective in cleavage-polyadenylation with only splicing elements remaining in the intron. Because we are able to see changes in sFlt-1 and Flt-1 mRNA expression in our mutated constructs, it can be concluded that the PPy tract is not optimal. Additionally, as Flt-1 mRNA decreases, a non-balanced reciprical increase in sFlt-1 mRNA is observed.

RNA Hybridization Assay

QPCR is a relatively new technique. Therefore, as a means of confirmation, the RNA hybridization assay was used. Although this assay can be less specific than QPCR, it allows the comparison of observed transcript sizes to those predicted by the composition of the expression construct. For Rep 1, an overnight upward/capillary transfer with Ambion®'s NorthernMax alkaline transfer buffer was successfully used to transfer both large and small mRNA species. However, concern for prolonged exposure to the alkaline conditions lead to the use of a brief pre-transfer alkaline treatment followed by neutralization and transfer in 20x SSC for Reps 2 and 3. Overnight capillary transfer using 20x SSC without the alkaline pre-treatment caused poor transfer of large mRNA species.

For each independent experiment, RNAs were separated via an agarose gel and transferred to a membrane. Each membrane was probed separately, with stripping between each probing. Binding locations of these probes can be seen in Figure 11. A representative blot for each probe is shown in Figure 13. The first probe (N-terminus "both" probe) was used in part to test the membrane stripping capabilities. Three bands are apparent in Figure 13A, one that migrates with the expected size of Flt-1, another which migrates with that of the predicted sFlt-1 transcript, and a third that remains unidentified. All three bands appear to vary in intensity across the mutations. Figure 13B shows a representative blot using the probe for Flt-1. Two bands are present here, one again corresponding to Flt-1 and another unexpected band. The largest variation in

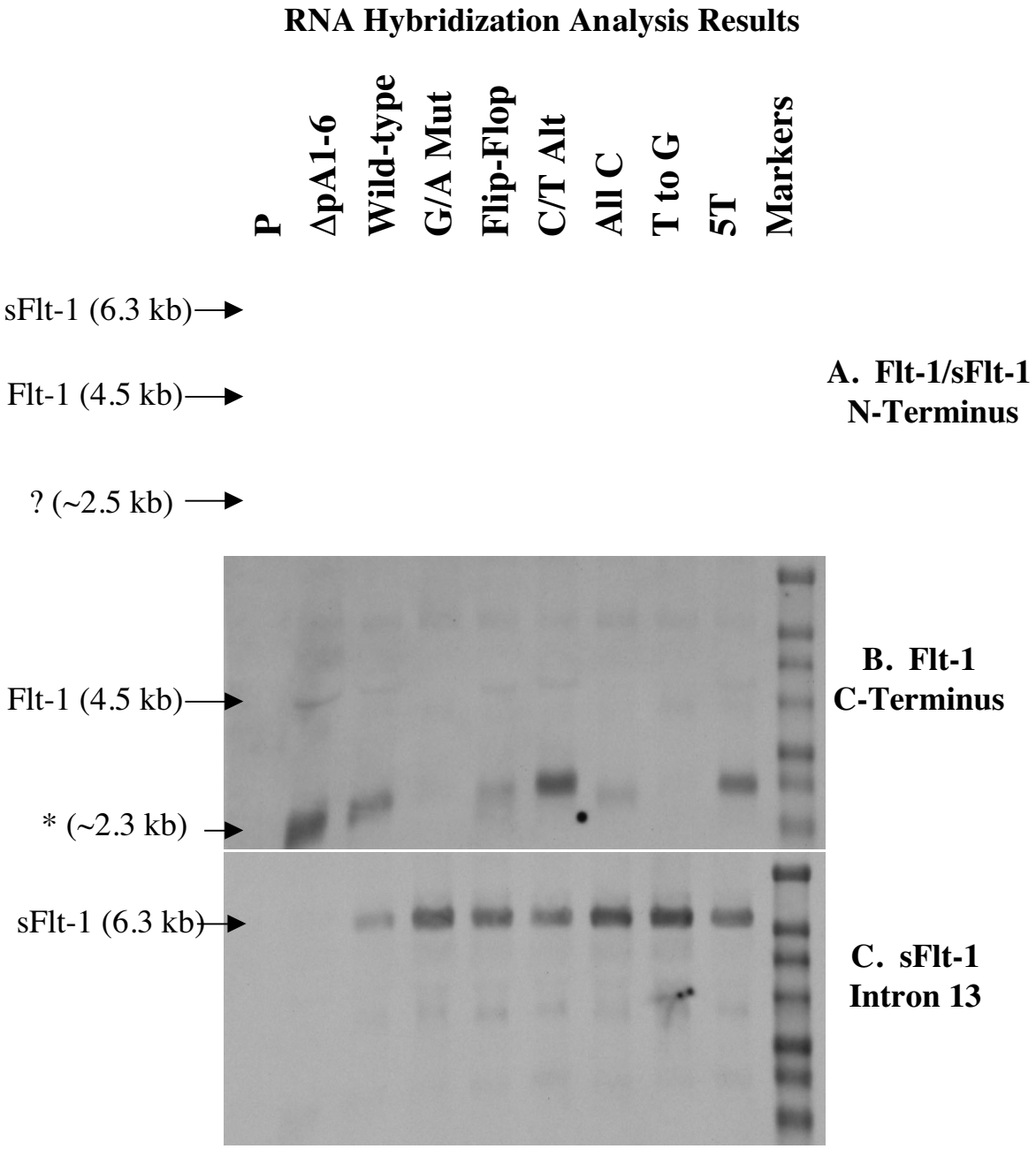

Figure 13 A, B, and C. RNA Hybridization Analysis Results. Differences in intensity can be seen across the lanes in each of these three blots. These support the results obtained in the QPCR. Identified band sizes are predicted based on known sequence and poly-adenylation sites. P = null vector. * This product is likely derived from splicing of the vector 5' UTR to the Flt-1 exon 14-30.

band intensity across lanes is evident on this blot. The pattern of intensity of the unexpected band parallels that of the Flt-1 band. Based on the apparent size of this unknown species (~2.3 kb), we speculated that it may represent an mRNA formed by the splicing of the 5'-UTR (untranslated region) directly to exon 14, instead of to exon 1 of Flt-1. The identity of this splicing variant (Figure 14) was confirmed through PCR (Primer sequences are listed in Appendix 1). Since this product does utilize the 3' splice acceptor from Flt-1 intron 13, we used this band as a substitute indicator of mutation effects on splicing efficiency in place of the less abundant Flt-1 band. The band that corresponds to sFlt-1 is the only one present in Figure 13C. Again, varying intensities can be seen across the lanes.

Densitometry was performed on each blot to estimate differences in Flt-1 and sFlt-1 expression that might stem from the PPy mutations. Three background samples were taken for each blot, and the means for each were subtracted from the densities for all bands of interest. Densitometry was done using the darker band from the unexpected Flt-1 splice variant (Figure 13B) as a surrogate for the exon 13-14 splice and the sFlt-1 band from Figure 13C. Direct statistical comparisons between band intensities for Flt-1 and sFlt-1 were not done because of the lack of internal normalization. Additionally, there is a possible influence of the PPy tract mutations on 5' splice site selection. As an alternative, band intensity data were rank-transformed and comparisons were made (Figure 15). As the mean rank for Flt-1 expression increases, the mean rank for sFlt-1 expression decreases. These results are consistent with those acquired from the QPCR: the mutations that showed relatively low Flt-1 expression were associated with relatively high sFlt-1 expression, and vice versa. This trend is also present in the raw data (not shown).

One drawback to the way this procedure was carried out was the lack of internal normalization of these results. Variation due to transfection and handling efficiency must be taken into consideration when the results are analyzed. One advantage to this assay is that it can show other splicing products to which the probes could bind. In this case, two unexpected bands were present in addition to the two expected mRNA forms. Overall,

results from this test support the conclusion that opposing trends are present in Flt-1 and sFlt-1 mRNA expression across the mutations.

Protein Immunoblotting

To determine whether the changes in steady-state mRNA levels described above were associated with changes in sFlt-1 protein accumulation, protein immunoblots were performed. Partially purified sFlt-1 from conditioned media in each of the three independent experiments were run on polyacrylamide gels and transferred to membranes. These membranes were then probed with an N-terminal Flt-1 antibody. This antibody could be used to detect sFlt-1 alone because the Flt-1 receptor is membrane bound and therefore is not present in the media. Each blot presented bands of differing intensities at about 100 kDa (the predicted size of sFlt-1). As with the RNA hybridization assay, background-corrected densitometry was done to estimate sFlt-1 protein levels derived from each transfection. Figure 16 contains both a representative blot and the table of results compiled from all three experiments. Background provided by the transfection host is minimal as shown by no detectable band in the lane for the plasmid-only control (P). As expected, the polyadenylation mutant (ΔpA1-6) shows a marked decrease in sFlt-1 protein expression. Again, G/A Mut, T to G, and the All C mutations show apparent increases in sFlt-1 protein levels, relative to the wild-type, that agree with the QPCR and RNA hybridization assay results. However, the mixed effects ANOVA with Tukey's HSD, indicated that none of the mean band intensities for the PPy mutants were statistically different from the wild-type. These results are not normalized to an internal control and therefore may reflect variability due to transfection, harvesting, and purification. Nevertheless, the apparent trend does support the conclusion that changes occur in the sFlt-1 protein that reflect those present in the sFlt-1 mRNA.

DISCUSSION

A secreted form of Flt-1, a receptor for the angiogenic growth factor VEGF, may influence responsiveness to VEGF. This sFlt-1 protein is produced from an mRNA species that retains part of intron 13 from the Flt-1 gene. In this project, we have tested the hypothesis that levels of sFlt-1 expression are, in part, determined by the efficiency of splicing mediated by the PPy tract of intron 13. Specifically, we attempted to make changes in sFlt-1 mRNA and protein expression levels by changing the PPy tract of Flt-1 intron 13. When the PPy tract sequence of intron 13 is compared to those of strong PPy tracts (48, 64), it can be predicted that the intron 13 PPy tract may be a suboptimal splicing signal. The intron 13 PPy tract is of a moderate length (16 nucleotides). However, when composition is examined, the PPy tract of intron 13 has only one stretch of three consecutive uridine residues, and an overall low uridine content (10:6, C:U). Because prior reports indicate that uridine is the preferred pyrimidine, altering the composition to favor uridine could have a profound affect on splicing.

Results obtained from this project support the importance of uridine content in the PPy tract. In three of the mutations created here, the uridine content was increased. Results from each of these mutations show an increase in Flt-1 mRNA expression. In the mutations where uridine content was reduced, either by changing to purines or in the All C mutation, there was a decrease in Flt-1 mRNA expression. Mutations were selected based on evidence of effective changes suggested by the literature. Roscigno *et al*. (55) published results of studies in which an adenovirus 2 intron was altered. Here they looked at *in vitro* splicing, the formation of splicing complexes, and the binding of proteins in HeLa nuclear extracts. In their initial experiments, they found that length and the composition of the PPy tract affected splicing and formation of splicing complexes. They began with a sequence rich in uridine residues. The mutations consisted of altering the fourth, seventh and/or tenth nucleotides in the sequence. Mutations which changed U→A in either the double or triple point mutant presented only 35% of the splicing product and low levels of the splicing intermediate (55). The mutants containing U→G changes did not splice detectably and showed only low levels of the splicing intermediates being formed (55). However, double mutants containing U→C changes

yielded 60-85% of the splicing product and high levels of the intermediate complexes (55). In these and other studies, it was found that a single purine substitution in a tract that was less than nine bases having fewer than five uridine residues consecutively had a detrimental effect on splicing (55, 57, 58, 65, 66). It was also shown that there is a strong preference for uridine residues over cytidine residues especially in tracts shorter than nine bases (55, 57, 58). Combining this information with that obtained from the results of the present study supports the conclusion that there is a required minimum number of uridines for the PPy tract to be functional.

In cells transfected with Flt-1 intron 13 PPy tract mutants that created a stretch of uridine residues four or greater, there was some increase in splicing (~2-fold maximum). However, these consecutive uridine residues did not have a dramatic impact on splicing efficiency, possibly because this tract is only 16 nucleotides long. The importance of the location of the consecutive uridine residues is supported by our results. In one mutation (5T), the uridine stretch is in the middle of the tract, eight bases from the 3' splice acceptor. In another mutation (Flip-flop), the uridine stretch is at the 5' end of the PPy tract, 15 bases from the 3' splice acceptor. In both cases there was a small increase in Flt-1 mRNA expression, but expression in the 5T mutant (1.9 x wild-type) was slightly greater than that in the Flip-flop mutation (1.2 x wild-type).

In another example from the literature, Coolidge *et al*. (57) found that composition and length of the PPy stretch affected splicing. In their experiment, a PPy stretch that consisted of varying G/U content was created. Most of the PPy tracts that were used were roughly 20 nucleotides in length. Strength of the PPy tract was determined in a splice-acceptor competition assay (57). In this experiment, a stretch of 17 guanosines prevented usage of the test tract completely, stretches of 17 and 23 uridine residues allowed usage nearly all the time, and a stretch of 16 cytidine residues allowed usage only 8% of the time (57). An alternating $(GU)_{11}$ PPy tract was used slightly more than half the time implying the need for uridine residues (57). It was also determined that the location and length of the uridine stretch has an effect on splicing. For stretches of greater than 10 uridine residues, the usage was minimally affected, but when the length of the uridine stretch was shortened to six, the location of the stretch is increasingly

important (57). As in the current studies, short stretches, closer to the 3' splice site, are used more efficiently while those closer to the branch point are used less frequently (57).

Results from the present project demonstrate a change in functionality in the mutations that either creates a continuous stretch of cytidine residues or an alternating C/T pattern. Contrary to the previous report (57), the alternating C/T mutation showed increased splicing efficiency (Flt-1 mRNA) while the All C mutation had decreased Flt-1 mRNA expression. Coolidge, *et al*. (57) also compared continuous stretches to alternating stretches of pyrimidines and found that the continuous stretches had an improved function. The difference here could also be due to the length of the PPy tract of Flt-1 intron 13. Additional experiments that would include altering the length of the Flt-1 intron 13 PPy tract as well as the uridine content could prove more conclusive.

One way that the content of the PPy tract could have an effect on splicing efficiency is by determining spliceosome protein binding affinity to the PPy tract, branch point, and/or 3' splice site. If there is competition between the spliceosome and the cleavage-polyadenylation machinery, as described for IgM mRNA processing, then an increased spliceosome binding affinity could effectively inhibit the cleavage-polyadenylation complex function, and more Flt-1 could be produced from a given pool of nascent Flt-1 pre-mRNA. Alternatively, if spliceosome protein binding is weakened, the balance could be shifted towards cleavage-polyadenylation and more sFlt-1 could be made. Adjusting this balance could have a profound effect on VEGF function by altering Flt-1 versus sFlt-1 isoform availability.

The results presented here support the idea that events of splicing and cleavage-polyadenylation may "compete" for Flt-1 pre-mRNAs. The apparent relative changes (increase or decrease) in the level of sFlt-1 mRNA production were small, whereas a wide range of Flt-1 mRNA expression could be seen across the mutations. If, as suggested by RNA hybridization results (Figure 13A), levels of sFlt-1 mRNA far exceed that of Flt-1 in the wild-type transfectants, then a large decrease in the number of Flt-1 mRNA copies upon mutation (eg. from 100→2 copies) would appear as a more profound percentage change than the reciprocal increase in copies of sFlt-1 mRNA (eg. from 500→598). Thus, in the G/A Mut, a greater than 100-fold decrease in Flt-1 mRNA was

associated with a less than 2-fold increase in sFlt-1 mRNA (Table 2). Another factor to consider is the more abundant Flt-1 splice variant produced (5' UTR to exon 14). If the amount of this product could be added to the amount of Flt-1 splicing product then maybe this total would be relatively equal to that of sFlt-1. If this is the case, then changes in Flt-1 may appear more comperable to those in sFlt-1.

In considering the effects of the mutations, it is important to note some of the limitations of these experimental procedures. QPCR is very specific. This is a benefit, but also a detriment. It allowed us to focus on specific targets of interest, but is not sensitive to other possible splicing variations. Fortunately, the RNA hybridization assay filled in this need. However, neither the RNA hybridization assay nor the protein immunoblot are as quantitative over so broad a dynamic range as QPCR, in part due to difficulties in normalization. At this point, sFlt-1, but not Flt-1, can be clearly detected by immunoblotting after transient transfection (75), so Flt-1:sFlt-1 protein ratios were not determined in the current study.

Little is known about the regulation of sFlt-1:Flt-1 ratios *in vivo*. In general, if sFlt-1 is produced at high levels, it can act to quench VEGF receptor mediated signaling by sequestering VEGF, reducing the total amount available to bind Flt-1 or the mitogenic receptor KDR. Increasing Flt-1 levels without altering sFlt-1 could have a profound affect on VEGF function. The inhibitory effect of sFlt-1 could become washed out, leading to increased angiogenesis. However, if Flt-1 levels were decreased while sFlt-1 remained unchanged, the functional effects of sFlt-1 would become more apparent, showing a reduction in angiogenic activity. When necessary, the body may increase VEGF and Flt-1 at constant sFlt-1, allowing a greater amount of VEGF to interact with Flt-1.

VEGF is not alone in its binding to Flt-1 and sFlt-1. PlGF, another Flt-1 ligand, weakly induces cellular proliferation and chemotaxis in addition to vascular permeability and angiogenesis (68, 71). Functional similarities between PlGF and VEGF are due in part to the selective binding of PlGF to Flt-1 (and sFlt-1) and its ability to form functional heterodimers with VEGF. However, activities of PlGF homodimer and PlGF/VEGF heterodimer have been shown to be much less than that of VEGF homodimers (68, 73).

Additionally, VEGF-B has been shown to compete with VEGF in its binding to the Flt-1 receptor (68). It is similar to PlGF in that it has multiple splice variants that differ in their heparin affinity, and it can also form heterodimers with VEGF. However, its tissue expression is wide, but most apparent in heart and skeletal muscle, suggesting that it may function as a homologue to PlGF in non-placental tissue (69). Nevertheless, it is likely that altering sFlt-1 availability would affect signaling by PlGF and VEGF-B as well as VEGF.

Adjusting VEGF activity by modulating sFlt-1 levels may offer an alternative to anti-VEGF antibody approaches currently being tested in clinical oncology trials. Altering ligand function pharmacologically via the receptors is a complex possibility. Normally, a balance is likely to be maintained to prevent over-expression or lack of function. It is important to consider systemic expression and function of these ligands and receptors. In the human female, menstrual cyclicity and pregnancy could be affected by changes in Flt-1 or sFlt-1 levels. This is not a problem in the male, but wound healing and other cardiovascular processes would increase complications here. Being able to localize alterations in Flt-1 or sFlt-1 expression would provide the ability to target the disease and not the patient. In addition, because Flt-1 and sFlt-1 are endogenous, concern about an immune response to immunoglobulin-based therapeutics is decreased. Another positive aspect to altering Flt-1 or sFlt-1 is that they represent the initial point in specific response pathways. Side effects from blocking downstream signal transduction elements involved in responses to numerous extracellular agents are less likely if the adjustment to the pathway is made at the beginning instead of the middle.

In this project, we demonstrate the intermediate strength of the Flt-1 intron 13 PPy tract through changes in sFlt-1 and Flt-1 expression levels caused by mutations of this region. The mutations made in this project did, in fact, lead to changes in mRNA levels for both sFlt-1 and Flt-1, and possibly sFlt-1 protein levels, supporting the idea that the PPy tract of intron 13 is of intermediate strength. The apparent reciprocity between sFlt-1 and Flt-1 mRNA production as illustrated by the PPy tract mutations, supports the hypothesis that the splice recognition sequences of intron 13, especially the polypyrimidine tract, are crucial for the regulation of sFlt-1 expression. However, this

story is far from complete. Several questions are raised that need to be addressed to achieve a more complete understanding of sFlt-1 expression. Specifically, future studies may examine how alterations in the PPy tract affect interactions with spliceosome proteins. It will be important to know what proteins are involved, how the described mutations interact with the cleavage-polyadenylation machinery, and whether extracellular conditions can affect splicing efficiency. We know that the PPy tract of Flt-1 intron 13 plays an important role in sFlt-1 and Flt-1 expression. The next question becomes how can we use this to our benefit.

REFERENCES

1. Folkman, J., and Y. Shing 1992. Angiogenesis. J Biol Chem. 267:10931-4.

2. Jaffe, R. B. 2000. Importance of angiogenesis in reproductive physiology. Semin Perinatol. 24:79-81.

3. Endo, T., Y. Kitajima, A. Nishikawa, K. Manase, M. Shibuya, and R. Kudo 2001. Cyclic changes in expression of mRNA of vascular endothelial growth factor, its receptors Flt-1 and KDR/Flk-1, and Ets-1 in human corpora lutea. Fertil Steril. 76:762-8.

4. Folkman, J. 1995. Angiogenesis in cancer, vascular, rheumatoid and other disease. Nat Med. 1:27-31.

5. Breier, G., A. Damert, K. H. Plate, and W. Risau 1997. Angiogenesis in embryos and ischemic diseases. Thromb Haemost. 78:678-83.

6. Richard, D. E., E. Berra, and J. Pouyssegur 1999. Angiogenesis: how a tumor adapts to hypoxia. Biochem Biophys Res Commun. 266:718-22.

7. Los, M., and E. E. Voest 2001. The potential role of antivascular therapy in the adjuvant and neoadjuvant treatment of cancer. Semin Oncol. 28:93-105.

8. Cotran, R. S., V. Kumar, T. Collins 1999. Robbins Pathologic Basis of Disease. W.B. Saunders Co., Philadelphia, p. 89-112, 260-327.

9. Bellamy, W. T., L. Richter, Y. Frutiger, and T. M. Grogan 1999. Expression of vascular endothelial growth factor and its receptors in hematopoietic malignancies. Cancer Res. 59:728-33.

10. Robinson, C. J., and S. E. Stringer 2001. The splice variants of vascular endothelial growth factor (VEGF) and their receptors. J Cell Sci. 114:853-65.

11. Neufeld, G., T. Cohen, S. Gengrinovitch, and Z. Poltorak 1999. Vascular endothelial growth factor (VEGF) and its receptors. Faseb J. 13:9-22.

12. Shibuya, M. 2001. Structure and function of VEGF/VEGF-receptor system involved in angiogenesis. Cell Struct Funct. 26:25-35.

13. Leung, D. W., G. Cachianes, W. J. Kuang, D. V. Goeddel, and N. Ferrara 1989. Vascular endothelial growth factor is a secreted angiogenic mitogen. Science. 246:1306-9.

14. Drake, C. J., A. LaRue, N. Ferrara, and C. D. Little 2000. VEGF regulates cell behavior during vasculogenesis. Dev Biol. 224:178-88.

15. Gale, N. W., and G. D. Yancopoulos 1999. Growth factors acting via endothelial cell-specific receptor tyrosine kinases: VEGFs, angiopoietins, and ephrins in vascular development. Genes Dev. 13:1055-66.

16. Epstein, S. E., R. Kornowski, S. Fuchs, and H. F. Dvorak 2001. Angiogenesis therapy: amidst the hype, the neglected potential for serious side effects. Circulation. 104:115-9.

17. Lee, Y. H., T. Tokunaga, Y. Oshika, R. Suto, K. Yanagisawa, M. Tomisawa, H. Fukuda, H. Nakano, S. Abe, A. Tateishi, H. Kijima, H. Yamazaki, N. Tamaoki, Y. Ueyama, and M. Nakamura 1999. Cell-retained isoforms of vascular endothelial growth factor (VEGF) are correlated with poor prognosis in osteosarcoma. Eur J Cancer. 35:1089-93.

18. Kim, K. J., B. Li, J. Winer, M. Armanini, N. Gillett, H. S. Phillips, and N. Ferrara 1993. Inhibition of vascular endothelial growth factor-induced angiogenesis suppresses tumour growth in vivo. Nature. 362:841-4.

19. Shiose, S., T. Sakamoto, H. Yoshikawa, Y. Hata, Y. Kawano, T. Ishibashi, H. Inomata, K. Takayama, and H. Ueno 2000. Gene transfer of a soluble receptor of VEGF inhibits the growth of experimental eyelid malignant melanoma. Invest Ophthalmol Vis Sci. 41:2395-403.

20. Plate, K. H., G. Breier, H. A. Weich, and W. Risau 1992. Vascular endothelial growth factor is a potential tumour angiogenesis factor in human gliomas in vivo Nature. 359:845-8.

21. Weidner, N. 1998. Tumoural vascularity as a prognostic factor in cancer patients: the evidence continues to grow. J Pathol. 184:119-22.

22. Siemeister, G., G. Martiny-Baron, and D. Marme 1998. The pivotal role of VEGF in tumor angiogenesis: molecular facts and therapeutic opportunities. Cancer Metastasis Rev. 17:241-8.

23. Hiratsuka, S., Y. Maru, A. Okada, M. Seiki, T. Noda, and M. Shibuya 2001. Involvement of Flt-1 tyrosine kinase (vascular endothelial growth factor receptor-1) in pathological angiogenesis. Cancer Res. 61:1207-13.

24. Pavco, P. A., K. S. Bouhana, A. M. Gallegos, A. Agrawal, K. S. Blanchard, S. L. Grimm, K. L. Jensen, L. E. Andrews, F. E. Wincott, P. A. Pitot, R. J. Tressler, C. Cushman, M. A. Reynolds, and T. J. Parry 2000. Antitumor and antimetastatic activity of ribozymes targeting the messenger RNA of vascular endothelial growth factor receptors. Clin Cancer Res. 6:2094-103.

25. Brekken, R. A., J. P. Overholser, V. A. Stastny, J. Waltenberger, J. D. Minna, and P. E. Thorpe 2000. Selective inhibition of vascular endothelial growth factor (VEGF) receptor 2 (KDR/Flk-1) activity by a monoclonal anti-VEGF antibody blocks tumor growth in mice. Cancer Res. 60:5117-24.

26. Clauss, M. 1998. Functions of the VEGF Receptor-1 (FLT-1) in the vasculature. Trends in Cardiovascular Medicine. 8:241-245.

27. Kroll, J., and J. Waltenberger 1997. The vascular endothelial growth factor receptor KDR activates multiple signal transduction pathways in porcine aortic endothelial cells. J Biol Chem. 272:32521-7.

28. Waltenberger, J., L. Claesson-Welsh, A. Siegbahn, M. Shibuya, and C. H. Heldin 1994. Different signal transduction properties of KDR and Flt1, two receptors for vascular endothelial growth factor. J Biol Chem. 269:26988-95.

29. Gerber, H. P., F. Condorelli, J. Park, and N. Ferrara 1997. Differential transcriptional regulation of the two vascular endothelial growth factor receptor genes. Flt-1, but not Flk-1/KDR, is up-regulated by hypoxia. J Biol Chem. 272:23659-67.

30. Shibuya, M. 2001. Structure and dual function of vascular endothelial growth factor receptor-1 (Flt-1). Cell Biol. 33:409-20.

31. Barleon, B., F. Totzke, C. Herzog, S. Blanke, E. Kremmer, G. Siemeister, D. Marme, and G. Martiny-Baron 1997. Mapping of the sites for ligand binding and receptor dimerization at the extracellular domain of the vascular endothelial growth factor receptor FLT-1. J Biol Chem. 272:10382-8.

32. Tanaka, K., S. Yamaguchi, A. Sawano, and M. Shibuya 1997. Characterization of the extracellular domain in vascular endothelial growth factor receptor-1 (Flt-1 tyrosine kinase). J Cancer Res. 88:867-76.

33. Cunningham, S. A., C. C. Stephan, M. P. Arrate, K. G. Ayer, and T. A. Brock 1997. Identification of the extracellular domains of Flt-1 that mediate ligand interactions. Biochem Biophys Res Commun. 231:596-9.

34. Davis-Smyth, T., H. Chen, J. Park, L. G. Presta, and N. Ferrara 1996. The second immunoglobulin-like domain of the VEGF tyrosine kinase receptor Flt-1 determines ligand binding and may initiate a signal transduction cascade. Embo J. 15:4919-27.

35. Kendall, R. L., and K. A. Thomas 1993. Inhibition of vascular endothelial cell growth factor activity by an endogenously encoded soluble receptor. Proc Natl Acad Sci U S A. 90:10705-9.

36. Kendall, R. L., G. Wang, and K. A. Thomas 1996. Identification of a natural soluble form of the vascular endothelial growth factor receptor, FLT-1, and its heterodimerization with KDR. Biochem Biophys Res Commun. 226:324-8.

37. Kondo, K., S. Hiratsuka, E. Subbalakshmi, H. Matsushime, and M. Shibuya 1998. Genomic organization of the flt-1 gene encoding for vascular endothelial growth factor (VEGF) receptor-1 suggests an intimate evolutionary relationship between the 7-Ig and the 5-Ig tyrosine kinase receptors. Gene. 208:297-305.

38. He, Y., S. K. Smith, K. A. Day, D. E. Clark, D. R. Licence, and D. S. Charnock-Jones 1999. Alternative splicing of vascular endothelial growth factor (VEGF)-R1 (FLT-1) pre-mRNA is important for the regulation of VEGF activity. Mol Endocrinol. 13:537-45.

39. Krussel, J. S., E. M. Casan, F. Raga, J. Hirchenhain, Y. Wen, H. Y. Huang, P. Bielfeld, and M. L. Polan 1999. Expression of mRNA for vascular endothelial growth factor transmembraneous receptors Flt1 and KDR, and the soluble receptor sflt in cycling human endometrium. Mol Hum Reprod. 5:452-8.

40. Goldman, C. K., R. L. Kendall, G. Cabrera, L. Soroceanu, Y. Heike, G. Y. Gillespie, G. P. Siegal, X. Mao, A. J. Bett, W. R. Huckle, K. A. Thomas, and D. T. Curiel 1998. Paracrine expression of a native soluble vascular endothelial growth factor receptor inhibits tumor growth, metastasis, and mortality rate. Proc Natl Acad Sci U S A. 95:8795-800.

41. Barleon, B., G. Siemeister, G. Martiny-Baron, K. Weindel, C. Herzog, and D. Marme 1997. Vascular endothelial growth factor up-regulates its receptor fms-like tyrosine kinase 1 (FLT-1) and a soluble variant of FLT-1 in human vascular endothelial cells. Cancer Res. 57:5421-5.

42. Siemeister, G., M. Schirner, K. Weindel, P. Reusch, A. Menrad, D. Marme, and G. Martiny-Baron 1999. Two independent mechanisms essential for tumor angiogenesis: inhibition of human melanoma xenograft growth by interfering with either the vascular endothelial growth factor receptor pathway or the Tie-2 pathway. Cancer Res. 59:3185-91.

43. Mahasreshti, P. J., J. G. Navarro, M. Kataram, M. H. Wang, D. Carey, G. P. Siegal, M. N. Barnes, D. M. Nettelbeck, R. D. Alvarez, A. Hemminki, and D. T. Curiel 2001. Adenovirus-mediated soluble FLT-1 gene therapy for ovarian carcinoma. Clin Cancer Res. 7:2057-66.

44. Crystal, R. G. 1999. In vivo and ex vivo gene therapy strategies to treat tumors using adenovirus gene transfer vectors. Cancer Chemother Pharmacol. 43:S90-9.

45. Chen, H., U. Ikeda, M. Shimpo, Y. Maeda, M. Shibuya, K. Ozawa, and K. Shimada 2000. Inhibition of vascular endothelial growth factor activity by transfection with the soluble FLT-1 gene. J Cardiovasc Pharmacol. 36:498-502.

46. Lear, A. L., L. P. Eperon, I. M. Wheatley, and I. C. Eperon 1990. Hierarchy for 5' splice site preference determined in vivo. J Mol Biol. 211:103-15.

47. Penotti, F. E. 1991. Human pre-mRNA splicing signals. J Theor Biol. 150:385-420.

48. Watakabe, A., K. Tanaka, and Y. Shimura 1993. The role of exon sequences in splice site selection. Genes Dev. 7:407-18.

49. Wagner, E. J., and M. A. Garcia-Blanco 2001. Polypyrimidine tract binding protein antagonizes exon definition. Mol Cell Biol. 21:3281-8.

50. Will, C. L., and R. Luhrmann 1997. Protein functions in pre-mRNA splicing. Curr Opin Cell Biol. 9:320-8.

51. Wu, J., and J. L. Manley 1989. Mammalian pre-mRNA branch site selection by U2 snRNP involves base pairing. Genes Dev. 3:1553-61.

52. Zhuang, Y. A., A. M. Goldstein, and A. M. Weiner 1989. UACUAAC is the preferred branch site for mammalian mRNA splicing. Proc Natl Acad Sci U S A. 86:2752-6.

53. Reed, R., and T. Maniatis 1988. The role of the mammalian branchpoint sequence in pre-mRNA splicing. Genes Dev. 2:1268-76.

54. Reed, R., and L. Palandjian 1997. Spliceosome assembly, p. 103-129. In A. R. Krainer (ed.), Eukaryotic mRNA Processing. IRL Press, Oxford.

55. Roscigno, R. F., M. Weiner, and M. A. Garcia-Blanco 1993. A mutational analysis of the polypyrimidine tract of introns. Effects of sequence differences in pyrimidine tracts on splicing. J Biol Chem. 268:11222-9.

56. Conte, M. R., T. Grune, J. Ghuman, G. Kelly, A. Ladas, S. Matthews, and S. Curry 2000. Structure of tandem RNA recognition motifs from polypyrimidine tract binding protein reveals novel features of the RRM fold. Embo J. 19:3132-41.

57. Coolidge, C. J., R. J. Seely, and J. G. Patton 1997. Functional analysis of the polypyrimidine tract in pre-mRNA splicing. Nucleic Acids Res. 25:888-96.

58. Bouck, J., S. Litwin, A. M. Skalka, and R. A. Katz 1998. In vivo selection for intronic splicing signals from a randomized pool. Nucleic Acids Res. 26:4516-23.

59. Singh, R., J. Valcarcel, and M. R. Green 1995. Distinct binding specificities and functions of higher eukaryotic polypyrimidine tract-binding proteins. Science. 268:1173-6.

60. Morris, D. R., T. Kakegawa, R. L. Kaspar, and M. W. White 1993. Polypyrimidine tracts and their binding proteins: regulatory sites for posttranscriptional modulation of gene expression. Biochemistry. 32:2931-7.

61. Garcia-Blanco, M. A., S. F. Jamison, and P. A. Sharp 1989. Identification and purification of a 62,000-dalton protein that binds specifically to the polypyrimidine tract of introns. Genes Dev. 3:1874-86.

62. Gil, A., P. A. Sharp, S. F. Jamison, and M. A. Garcia-Blanco 1991. Characterization of cDNAs encoding the polypyrimidine tract-binding protein. Genes Dev. 5:1224-36.

63. Tazi, J., C. Alibert, J. Temsamani, I. Reveillaud, G. Cathala, C. Brunel, and P. Jeanteur 1986. A protein that specifically recognizes the 3' splice site of mammalian

pre-mRNA introns is associated with a small nuclear ribonucleoprotein. Cell. 47:755-66.

64. Peterson, M. L. 1992. Balanced efficiencies of splicing and cleavage-polyadenylation are required for mu-s and mu-m mRNA regulation. Gene Expr. 2:319-27.

65. Patterson, B., and C. Guthrie 1991. A U-rich tract enhances usage of an alternative 3' splice site in yeast. Cell. 64:181-7.

66. Norton, P. A. 1994. Polypyrimidine tract sequences direct selection of alternative branch sites and influence protein binding. Nucleic Acids Res. 22:3854-60.

67. Frendewey, D., and W. Keller 1985. Stepwise assembly of a pre-mRNA splicing complex requires U-snRNPs and specific intron sequences. Cell. 42:355-67.

68. Clauss, M. 2000. Molecular biology of the VEGF and the VEGF receptor family. Semin Thromb Hemost. 26:561-9.

69. Olofsson, B., E. Korpelainen, M. S. Pepper, S. J. Mandriota, K. Aase, V. Kumar, Y. Gunji, M. M. Jeltsch, M. Shibuya, K. Alitalo, and U. Eriksson 1998. Vascular endothelial growth factor B (VEGF-B) binds to VEGF receptor-1 and regulates plasminogen activator activity in endothelial cells. Proc Natl Acad Sci U S A. 95:11709-14.

70. Ahmed, A., C. Dunk, S. Ahmad, and A. Khaliq 2000. Regulation of placental vascular endothelial growth factor (VEGF) and placenta growth factor (PIGF) and soluble Flt-1 by oxygen--a review. Placenta. 21 Suppl A:S16-24.

71. Clauss, M., H. Weich, G. Breier, U. Knies, W. Rockl, J. Waltenberger, and W. Risau 1996. The vascular endothelial growth factor receptor Flt-1 mediates biological activities. Implications for a functional role of placenta growth factor in monocyte activation and chemotaxis. J Biol Chem. 271:17629-34.

72. Lewin, B. 2000. Genes VII. Oxford UP: New York. p. 685-718.

73. Davis-Smyth, T., L.G. Presta, and N. Ferrara 1998. Mapping the charged residues in the second immunoglobulin-like domain of the vascular endothelial growth factor/placenta growth factor receptor Flt-1 required for binding and structural stability. J Biol Chem. 273:3216-22.

74. Ishii, T.M., P. Zerr, X. Xia, C.T. Bond, J. Maylie, and J.P. Adelman 1998. Site-directed mutagenesis. Meth in Enzymol. 293:53-71.

75. Huckle, W.R., and R.I. Roche 2002. Multiple cleavage-polyadenylation sites in processing of mRNA for soluble Flt-1, an endogenous inhibitor of VEGF signaling. Submitted.

APPENDICES

Appendix A. Primer Sequences

Sequencing and PCR Primer Sequences

M13-Forward- GTAAAACGACGGCCAGT
M13-Reverse- AACAGCTATGACCATG
BH-204, AGGGCACTGGGCTTTCTTATTAC
BH-205, AGAAGACTCGGGCACCTATG
BH-206, GGCGCGGGGACACCTCTA
BH-216, AAGATGCCAGCCGAAGGAGAGGAC
BH-217, CTTTAGGCGGGCGGGGAGGAGTA
BH-220, GGTCTCCATCAGTGGCTCTACGACCTT
BH-226, GAATTATGAAGGTCCAGCAGGTCT
BH-227, CCCAGGGGCCATGAGTGTTTA
BH-238, CTCTGGATTTCTGCCCTAGGATTTGC
BH-239, GAAGTGTAGACTATGGAGTAACACAACC
BH-242, AACCAGCACTTCCTTCAACGCGTG
BH-244, AGTTGTCTGGGCACTGTTGAATGCT
BH-245, GTTATCACGTTTTCTTAAGGGAAGCC
BH-247, AGGAACGGCAGTACCCTCCA
BH-257, GAGCTTCCAGAATGAAAATGTGGA

Taqman® Primer and Probe Sequences

sFlt-1
BH-211, GGGAAGACATCCTTCGGAAGA
BH-212, TCCGAGAGAAAATGGCCTTTT
BHTP-1, 6FAM-CCGCAGTGCTCACCTCTAACGAGAACTTCT-TAMRA

Flt-1
BH-228, TTCGGAAGACAGAAGTTCTCGTT
BH-229, GACCTCGTAGTCACTGAGGTTTTG
BHTP-3, 6FAM-AGATTCGGAAGCGCCACACCTGCT-TAMR

neo^r
BH-296, GCGCCCGGTTCTTTTTGT
BH-297, GCCTCGTCCTGCAGTTCATT
BHTP-5, FAM-AAGACCGACCTGTCCGGTGCCCT-TAMRA

Appendix B. Common Kits/Products Used

Ambion®, Austin, TX

BrightStar™ Psoralen-Biotin Nonisotopic Labeling Kit
Catalog #1480
NorthernMax™ Formaldehyde-Based System for Northern Blots
Catalog #1940
BrightStar™ Biotinylated RNA MillenniumTM Markers
Catalog #7170
BrightStar™BioDetect™ Nonisotopic Detection Kit
Catalog #1930
RETROscript™ First Strand Synthesis Kit for RT-PCR
Catalog #1710

Life Technologies™, Carlsbad, CA

T4 DNA Ligase
1 unit/µl
Catalog #15224-017
T4 DNA Ligase Buffer (supplied with T4 DNA Ligase)
50mM Tris-HCl (pH 7.6)
10mM $MgCl_2$
1mM ATP
1mM DTT
5% (w/v) polyethylene glycol-8000
Store at –20°C
S.O.C. Medium
2% Tryptone
0.5% Yeast Extract
10mM NaCl
2.5mM KCl
10mM $MgCl_2$
10mM $MgSO_4$
20mM Glucose
Catalog #15544-034

New England Biolabs, Beverly, MA (Restriction endonuclease buffers)

NEBuffer EcoRI (1x)
50mM NaCl
100mM Tris-HCl
10mM $MgCl_2$
0.025% Triton X-100
pH 7.5 @ 25°C

NEBuffer 2 (1x)
50mM NaCl
10mM Tris-HCl
10mM $MgCl_2$
1mM dithiothreitol
pH 7.9 @ 25°C

NEBuffer 3 (1x)
100mM NaCl
50mM Tris-HCl
10mM $MgCl_2$
1mM DTT
pH 7.9 @ 25°C

NEBuffer 4 (1x)
50mM potassium acetate
20mM Tris acetate
10mM magnesium acetate
1mM DTT
pH 7.9 @ 25°C

Bovine serum albumin (BSA)
Supplied by NEB with the enzymes.

QIAGEN®, Valencia, CA

QIAEX® II Gel Extraction Kit
Catalog #20021

QIAGEN® Plasmid Purification Midi Kit
Catalog #12143

RNeasy® Mini Kit
Catalog #74104

QIAshredder Homogenizers
Catalog #79654

RNase-Free DNase Set
Catalog #79254

Taq Polymerase Master Mix Kit
Catalog #201443

Appendix C. Other Buffers and Equipment.

PCR Reagents

Pfu Turbo® DNA Polymerase 2.5 units/µl
Stratagene, Catalog #600250

10x Cloned *Pfu* DNA Polymerase Reaction Buffer (Provided with Polymerase)
200mM Tris-Hcl (pH8.8)
20mM $MgSO_4$
100mM KCl
100mM $(NH_4)_2SO_4$
1% Triton® X-100
1mg/ml Nuclease-Free BSA

TaqMan® Universal PCR Core Kit
PE Biosystems,Catalog #4304437

Reagent	Supplied Concentration		Final Concentration
10x buffer A	10	x	1.0
MgCl2	25	mM	3.50
dATP	10	mM	0.20
dCTP	10	mM	0.20
dGTP	10	mM	0.20
dUTP	20	mM	0.40
5' primer*	10	uM	0.30
3' primer*	10	uM	0.30
Probe*	100	uM	0.20
AmpliTaq Gold	5	U/ul	0.025
AmpErase UNG	1	U/ul	0.010

* Gene specific. Sequences appear in Appendix A.

Membranes

RNA Hybridization:
Zeta-Probe® GT Genomic Tested Blotting Membranes
Catalog #162-0197
Protein Immunoblot:
Immobilon™ –P Transfer Membrane
Catalog #IPVH00010

Buffers

RNA Hybridization

Transfer Buffer (20x SSC)
- 0.3M sodium citrate dihydrate
- 3.0M sodium chloride
- pH 7.0 @ 23ºC
- Fisher Biotechnology Catalog #BP1325-4

Protein Immunoblot:

Tank Buffer
1x SDS PAGE diluted (10x stock)
- 10X SDS PAGE STOCK (Fisher BP1341-1)
  - 0.25M Tris base
  - 1.92M Glycine
  - 1% SDS weight /volume

Transfer Buffer
10% MeOH Total Vol: 500mls
- 50ml 10x – 0.25M Tris base + 1.92M glycine
- 400ml H_2O
- 50ml Methanol
- Let stand to remove air bubbles.

TNT
1x TNT from 10x TN
- 900ml H_2O
- 100ml 10x TN (250mM Tris-Cl + 1500mM NaCl, pH 7.5)
- 5ml 10% Tween 20

Blocking Buffer
0.2% gelatin in 50ml 1x TNT
- 0.1g gelatin
- 50ml TNT
- Microwave at 30% power for short times until dissolved. Refrigerate.

Agarose Gel Electrophoresis:

Running Buffer
1x TBE from 10x
- 0.89M Tris
- 0.87M Boric Acid
- 0.027M EDTA

Gel Loading Solution

0.05% (w/v) Bromphenol blue
40% (w/v) Sucrose
0.1 M EDTA, pH 8.0
0.5% (w/v) Sodium lauryl sulfate (SDS)
Suitable for use in nucleic acid gel electrophoresis. Store at room temperature.

Cell Culture and Transfection Reagents:

DMEM/FBS/Gent:

Dulbecco's Modified Eagle Medium (DMEM) with 4.5 mg/ml glucose, glutamine (Mediatech #10-013-CV) containing
10% (v/v) Fetal Bovine Serum (Mediatech #14-501-F)
50 ug/ml Gentamycin (LTI #15710-072).
In hood, combine sterile liquid components in DMEM bottle using sterile pipets. Store at 4°C.

DPBS:

Dulbecco's Phosphate Buffered Saline, Ca^{2+}/Mg^{2+}-free
(Mediatech #21-031-CM).
Store at room temperature.

Trypsin/EDTA (1X)

0.5 mg/ml Trypsin
0.2 mg Na_4EDTA in DPBS (10X as Sigma T-4174).
Dilute to 1X, filter sterilize, and aliquot by 40 ml into sterile conical polypropylene tubes. Store –20°C long-term; 4°C short-term.

Other

Luria-Bertani (LB)Broth, dehydrated

10g/L Bacto Tryptone
5g/L Bacto Yeast Extract
10g/L Sodium Chloride
Becton Dickinson # 244620

Luria-Bertani (LB) Agar, dehydrated

10g/L Bacto Tryptone
5g/L Bacto Yeast Extract
10g/L Sodium Chloride
15g/L Bacto Agar
Becton Dickinson # 244520

Tris-EDTA (TE)

1M Tris-HCl
0.1M EDTA
pH 8

Sequencing

Automated DNA sequencing was performed in the Core Laboratory Facility at the Virginia Bioinformatics Institute using standard methods on an ABI 377 automated DNA Sequencer or an ABI 3100 capillary sequencer and using Applied Biosystems BigDye (version 2.0) Terminator chemistry.

Cycle sequencing reactions were performed using 10 ng/100 bp of PCR product (or if plasmid template, 500 ng total) and Applied Biosystems (Foster City CA) Big Dye Terminator (version 2.0) ready reaction kit.

Primer amount in the reaction was 3.2 pmol

Total reaction volume was 15ul

Cycling parameters were: 30 cycles of 30 sec @ 95ºC, 15 sec @ 50ºC, 4 min @ 60ºC and refrigerated until used.

Reactions were purified using the Millipore Multiscreen plates and dried and resuspend as per manufacturer's protocols for loading on the automated sequencer.

Appendix D. GM2163 cell competency protocol

1. Streak LB-chloramphenicol plate with GM2163 cells, incubate overnight at 37^{o}C.
2. Pick colony to inoculate 10 ml culture of LB broth, incubate overnight at 37^{o}C with shaking, 250 rpm.
3. Dilute 1 ml from 10 ml suspension to 100 ml LB broth and incubate at 37^{o}C with shaking, 250 rpm approximately 2 hours.
4. At intervals, remove sample and read absorbance at 590 nm.
5. When A_{590} is between 0.375 and 0.400, transfer suspension to 2-50 ml tubes and incubate on ice for 10 minutes.
6. Centrifuge at 1,600 x g for 10 minutes at 4^{o}C (no brake).
7. Remove supernatant and resuspend each pellet in 10 ml chilled, sterile 100 mM $CaCl_2$.
8. Centrifuge at 1,100 x g for 5 minutes at 4^{o}C (no brake).
9. Remove supernatant, and resuspend each pellet in 10 ml chilled, sterile 100 mM $CaCl_2$, incubate on ice for 30 minutes.
10. Centrifuge at 1,100 x g for 5 minutes at 4^{o}C (no brake).
11. Remove supernatant and resuspend each pellet in 2 ml chilled, sterile 100 mM $CaCl_2$.
12. Pool and store at 4^{o}C. Use within 2-3 days.

Appendix E. Thermocycler Programs

Program 1: Used unless otherwise stated for PCR reactions

Stage	Step	Temperature (°C)	Time (minutes)	# Cycles
1	1	94	2	1
	2	60	1	
	3	72	2	
	4	0	0	
2	1	94	1	28
	2	60	1	
	3	72	2	
	4	0	0	
3	1	94	1	1
	2	60	1	
	3	72	10	
	4	0	0	
4	1	4	Hold	N/A
			Total Cycles:	30

Program 2: Used for creating mutations in both rounds of PCR.

Stage	Step	Temperature (°C)	Time (minutes)	# Cycles
1	1	94	2	1
	2	55	1	
	3	72	2	
	4	0	0	
2	1	94	1	18
	2	55	1	
	3	72	2	
	4	0	0	
3	1	94	1	1
	2	55	1	
	3	72	10	
	4	0	0	
4	1	4	Hold	N/A
			Total Cycles:	20

VITA

Rebecca I. Roche

Rebecca I. Roche was born to Timothy and Nancy Roche in May of 1978 in Bloomsbury, NJ. With a strong 4-H background and high school behind her, she proceeded to Virginia Tech for her undergraduate work. As a senior, she worked with Dr. Stephen Boyle on an undergraduate research project involving immunocontraception in the feline. She completed her undergraduate work in 2000 at Virginia Polytechnic Institute and State University, earning Bachelor of Science degrees in Biochemistry and Animal and Poultry Science. Continuing with her education, she entered the Veterinary Medical Science program as a Master's of Science candidate under Dr. William R. Huckle. Educational funding was provided as Research/Teaching Assistantships. In this capacity she worked at the Virginia Tech DNA Sequencing Facility under Lee Weigt and Nickole Kaufman and assisted Dr.s M. Ehrich and H. Bender in Veterinary Pharmacology and Clinical Pathology classes, respectively. When she is not working or doing research, Rebecca enjoys playing with her horse and oil painting.